# An Experimental Framework for Outdoor E-band Millimeter Wave Transmission Evaluation

by

YaYa Brown

A Thesis
Submitted to the Faculty
of the
WORCESTER POLYTECHNIC INSTITUTE
in partial fulfillment of the requirements for the
Degree of Master of Science
in
Electrical and Computer Engineering
by

May 2021

APPROVED:

Dr. Alexander Wyglinski, Research Advisor

Dr. Douglas Petkie, Committee Member

Dr. Reinhold Ludwig, Committee Member

# Abstract

In this thesis, a custom-built millimeter wave testbed for evaluating out-of-beam energy emissions in the E-band frequencies (71-76 GHz) is presented. Millimeter wave-based communication systems are gaining attention due to the increased demand for fast and reliable wireless connection. The electromagnetic and propagation properties for signals at these higher frequencies require additional research for determining the best system configuration for future applications. This project develops an experimental custom-built hardware framework for studying outdoor E-band transmissions and assessing received signal power using relatively inexpensive hardware components that can be customized to any application. Received signal power measurements were completed at 71.9375 GHz, as a proof-of-concept for the testbed. The results indicated that signals can be detected even when misalignment of the transmit and receive antennas occur.

# Acknowledgements

I would like to thank Professor Wyglinski for going above and beyond in helping me complete this project. From setting up all the hardware for the testbed at his house to providing his invaluable advice, Professor Wyglinksi was truly an amazing advisor. I want to thank Professor Petkie and Professor Ludwig for serving on my committee and offering their advice and suggestions in regards to my thesis. I would like to acknowledge the support from MIT Lincoln Laboratory and the helpful advice from Carl, Sia, and Devin. I also want to thank Mr. Hanson for his help in building the enclosures for the testbed. I want to thank Juli for helping me edit this thesis. I want to thank all my friends for their support. Lastly, I would like to thank my parents for their constant love and support.

# Contents

# List of Figures

# List of Tables

# Chapter 1

# Introduction

## 1.1 Motivation

Technology in the wireless communication industry is rapidly growing in order to accommodate the demand for reliable and fast connection. According to Pew Research Center, 90% of Americans use the Internet, and an increasing number of people are using their smartphones as a means to go online as opposed to traditional broadband [1], [2]. Along with a rising number of Internet users, there is also a growing dependence on Internet access that has been highlighted by the ongoing event of the COVID-19 pandemic. 53% of Americans have reported that the Internet has been essential to their everyday life during these times [3]. Outside of the events of the pandemic, the Internet's role in society continues to expand. In the sphere of education, 35% of American students have engaged in some type of distance learning at the postsecondary level, with 16.6% of them exclusively taking distance learning courses [4]. The Internet has also affected healthcare; for example, it enables faster access of patient information, facilitates the collaboration between healthcare providers, and allows patients to remotely receive care [5]. As the Internet impacts many aspects of people's lives, the technology needs to be researched and developed to give people reliable and fast access to it.

Current wireless communication technology uses frequency bands that are below 6 GHz for consumers. The growing demand for capacity and an increasing number of users means

that the available bandwidth will not be enough to enable the kind of connection that users will want or need. A solution to this issue is to use millimeter wave frequency bands to communicate due to their large amount of available bandwidth. The use of millimeter waves has already begun with the beginning rollout of 5G; two major cell phone service providers in the United States, Verizon and AT&T, have incorporated millimeter wave technology into their 5G rollout plans [6], [7].

In order to further develop the technology to utilize millimeter waves, there needs to be more research performed in this area to both create technology and determine potential points of vulnerability. Millimeter wave signals have fundamentally different properties than the traditional radio frequency bands that have been widely used for communication. They also have more limitations; radio frequency bands have smaller communication ranges, need a clear line of sight for the best connections, and are easily blocked by such common things such as buildings, glass and foliage [8]. Therefore, creating technology in these bands requires research into these properties. As the world becomes more digitally-dependent, there is a growing need for security measures—even at the physical layer—which could look different than those of radio frequency bands. The current equipment that operates in millimeter wave bands, especially at higher frequencies, is relatively expensive, which limits accessibility to this type of research.

## 1.2 Current State-of-the-Art

In the open literature, most of the focus for wireless communications has been on the lower frequencies of the millimeter wave spectrum, mainly 20-40 GHz as well as 60 GHz, despite that the spectrum spans up to frequencies of 300 GHz [9]. This discrepancy is largely due to the limited amount of affordable and customizable equipment found in the higher frequencies. It is also due to some of those ranges already being allocated, such as 76-81 GHz, which is used for short-range vehicular radar applications [10]. The 60 GHz range is currently unlicensed; this makes research more accessible and equipment more readily available, as applying for a license from the FCC is not necessary.

Propagation measurements and channel models have been researched in the following

frequencies: 28 GHz, 38 GHz, 60 GHz, and 73 GHz [9]. These experiments were made with transmitters and receivers that used a double conversion superheterodyne RF architecture and an attached steerable pyramidal horn antenna in order to make outdoor propagation measurements and channel models for five different cellular scenarios [11].

There is a relatively large amount of completed research and testbeds in the 60 GHz range because it is an unlicensed band. One testbed was created using a basic RF front end from Pasternack components and software defined radio (SDR) technology to collect the data to make a millimeter wave testbed with the addition of noise cancellation because in those transceivers the high oscillation frequency causes noise [12]. Another utilized WiGig transceivers but was more focused on the networking involved in edge content delivery [13]. Due to their highly directional beams, millimeter wave signals are often thought of as extremely difficult to eavesdrop on. However, using 60 GHz transceivers, researchers were able to place objects in such a way to reflect signals to facilitate eavesdropping [14]. There has also been research completed that found millimeter wave signals to be susceptible to side lope attacks, and the testbed that was used included phased array antennas and development boards for the transmitter and receiver [15]. There are numerous testbeds and research efforts currently underway into 60 GHz; however, this band suffers from high oxygen attenuation and will not be able to be used in every application.

Overall, there are a few key considerations missing from the current testbeds being used. Firstly, most of the testbeds are either expensive or made for specific experiments and can not be easily replicated and customized to serve many research purposes. Secondly, most of the research is focused on the lower frequency bands with few looking at the 70 GHz range. Thirdly, the out of beam emissions and vulnerabilities of the higher frequency bands above 60 GHz have not been researched extensively.

## 1.3 Thesis Contributions

The goal of this thesis was to create a relatively inexpensive testbed, in the 71-76 GHz range, that could serve as a framework to enable future research into potential vulnerabilities, use cases, and new technology for millimeter wave wireless communications. Figure 1.1

gives a conceptual diagram of the contributions.

A. A permanent outdoor millimeter testbed that consisted of four radios that were able to communicate data between two sets of communication links.

B. A custom-built wireless millimeter wave measurement platform that utilizes basic hardware components. It outputs data to a spectrum analyzer to enable the visualization of signals. This is a basic framework that can be modified for different purposes.

C. An initial proof-of-concept series of controlled experiments analyzing out-of-beam wireless emissions at 71.9375 GHz.

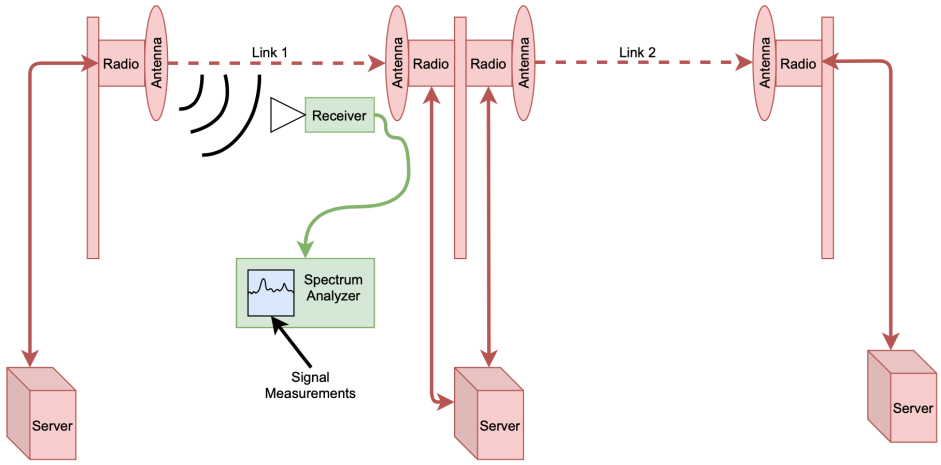


Figure 1.1: Thesis contribution A's elements are colored red, contribution B's elements are colored green, and contribution C's element is colored blue.

## 1.4 Thesis Organization

This thesis is organized as follows: Chapter 2 gives an overview of millimeter wave properties, propagation measurements, and general RF component explanations. Chapter 3 details the testbed configuration for four commercial millimeter wave radios in an outdoor

environment. Chapter 4 presents the hardware framework for a 71-76 GHz sensor unit. Chapter 5 includes the initial measurement results. Chapter 6 is a summary of the thesis and gives suggestions for areas of improvement for this testbed.

# Chapter 2

# Brief Millimeter Wave Communications Overview

Millimeter wave (mmWave) signals are defined by the size of their wavelengths, which range from 10 mm to 1 mm, and the span of their frequency which is between 30 GHz to 300 GHz [16]. The smaller wavelength size causes certain signal attenuation properties that are not prevalent in lower frequency bands used for commercial communications. This chapter goes into detail about signal attenuation caused by the atmosphere, rain, foliage, fog, and different building materials. An explanation of how the fundamental elements of a receiver operating in mmWave frequencies will also be covered.

## 2.1 Physical Properties of Millimeter Wave Signals

In wireless communications, a fundamental form of attenuation called free space path loss exists for all signals [17]. This is due to the physical properties of a signal as it travels out from a transmitter into free space. It is defined as the power dispersion of a signal as it travels to a receiver, and is expressed as the ratio of the transmit power to the received power [17]:

$$L = \frac{P_t}{P_r} = \frac{(4\pi d)^2}{\lambda^2},$$

where $\lambda$ is the wavelength of the signal and $d$ is the distance between the transmitter and receiver, both in the unit of meters. A modification can be made to this equation since wavelength can be expressed as the speed of light divided by frequency of the signal $\lambda = c/f$ [18]:

$$L_{dB} = 20log_{10}(\frac{4\pi fd}{c}),$$

where $f$ is the frequency of the signal and $c = 3 * 10^8\, m/s$ is the speed of light.

If two signals are transmitted across one meter and one is being transmitted at a frequency of 30 GHz and the other at 3 GHz, we can compare the free space path loss of these two signals using the above equation. The 3 GHz signal power is approximately $\frac{1}{125}$ of its original transmit power which can also be expressed as a power loss of 42 dB. The 30 GHz signal power is approximately $\frac{1}{1250}$ of its original transmit power which can also be expressed as a power loss of 62 dB. This shows there is an additional order of magnitude of transmit power loss when comparing the two signals. This demonstrates the extent to which mmWaves are affected by free space path loss. However, this is just one of many different potential sources of attenuation that mmWave signals experience.

Free space path loss occurs as a result of how signals travel. The medium that they travel in, however, will also cause some form of attenuation from the atmosphere and the different elements within it. If the medium is air, then the location where a mmWave communication link is set up has to be carefully considered, as altitude, pressure, temperature, water vapor density, and the angle between the transmitter and receiver can all cause an increase in signal strength loss [19]. For instance, attenuation at one meter in decibels is shown for frequencies from 1 GHz to 300 GHz in Figure 2.1 for both low and high altitudes.

Rainfall is another factor that impacts mmWave communications, particularly more than those at lower frequencies. This is because the higher frequency mmWave signals have wavelengths that are small enough to be similar in size to the droplets, which causes the signal to be absorbed, scattered, depolarized, and diffracted, more so than when the wavelengths are much larger [22]. The size and orientation of the droplets can cause differing amounts of over-the-air attenuation [23]. An increased rate of rainfall will cause more signal attenuation as a result of the droplets becoming larger, and in some cases can cause the communication link to go down [22]. The rate of rainfall is not uniform across a

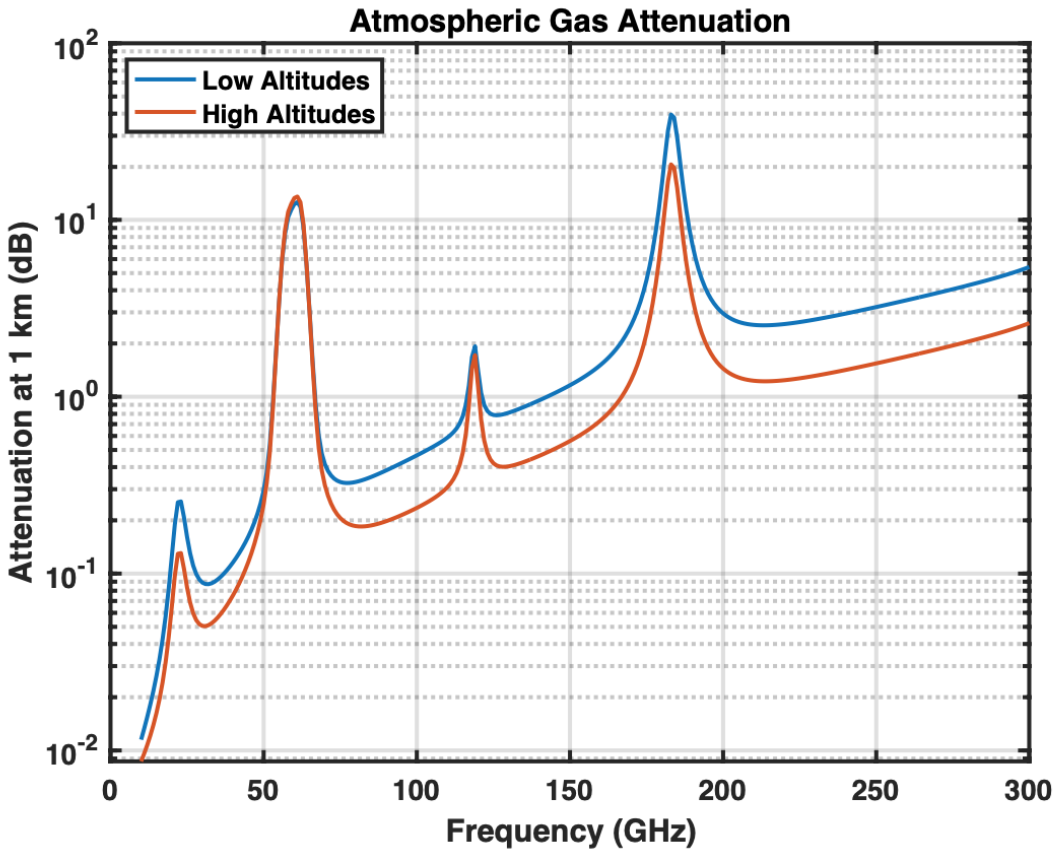


Figure 2.1: The atmospheric gas attenuation curves generated using code from [20] based on formulas from [19]. The peaks of attenuation, at various frequencies, are due to the absorption of energy from water vapor (22 GHz) and oxygen (60 GHz) [21].

communication link because rain spatially varies [24]. There are currently two models for rain attenuation; the ITU-R P.530-17 [25] and Crane [26] models, which are compared in Figure 2.2.

Snow and fog can also affect the communication link for mmWave signals, as both increase the amount of water vapor in the air and consequently hinder the signal. Two different types of fog were studied: radiation and advection. Radiation fog is formed in the evening when the heat that was absorbed in the Earth during the day is radiated into the air, and advection fog is created when warm, moist air passes over a cold surface,

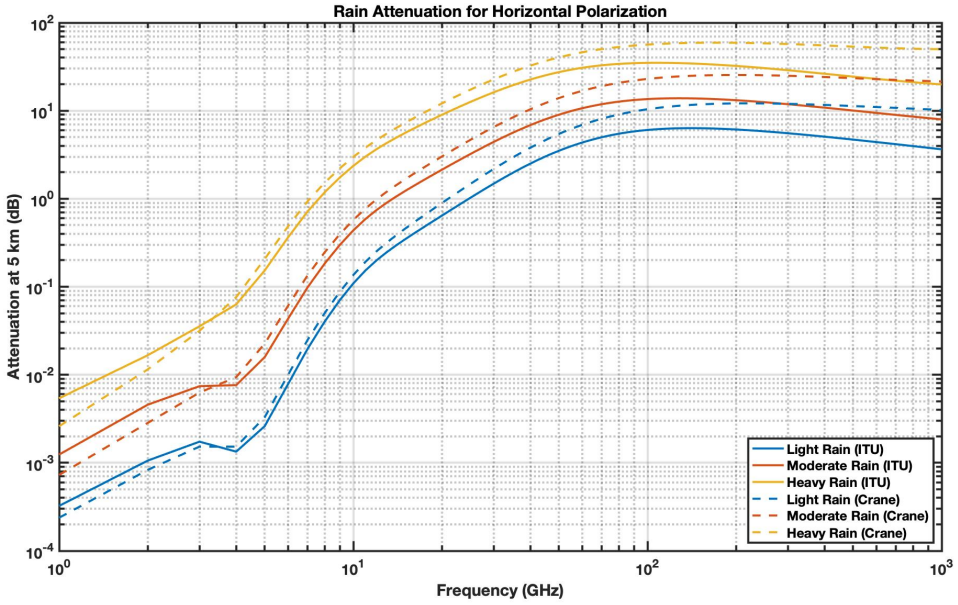


Figure 2.2: The rain attenuation curves generated using code from [20] based on formulas from [25] and [26]. Light, moderate, and heavy rain are being defined as rainfall rates at 1 mm/hr, 4mm/hr, and 20 mm/hr respectively. Different considerations must be made for tropical environments due to the increased amount of rain in comparison to other parts of the world [24].

causing water vapor to condense and form fog [27]. Studies have found that there can be a difference of 8 dB/km attenuation between advection and radiation fog; however, signal scattering occurs less with fog than with rain, as the droplet sizes of fog are much smaller than those of rain [28]. Snow, when its snowflakes are similar in size to or larger than the wavelengths of a signal, can cause scattering [29]. The most likely determinant in how much signal attenuation has occurred is the water content percentage of the snow [30], [28].

The location of where a communication link is set up can influence the maximum distance between transmitters and receivers in areas that are more likely to experience attenuation, as it would be beneficial to reduce the distance between transmitters and receivers to ensure quality performance despite varying conditions in areas that experience more weather. In addition to a location's atmospheric and weather dependent qualities, surrounding struc-

tures and general area must also be considered. Foliage loss, which is signal attenuation due to vegetation, poses an issue for mmWave signals since they can become absorbed and scattered due to the branches, leaves, and trunks of trees. Since mmWave frequencies cover a large range, it is important to note that the following data was obtained with experiments at 9.6 GHz, 28.8 GHz, and 57.6 GHz. The experiments concluded that at distances below 30 m through an orchard, foliage attenuation was observed to be 1.3 dB/m to 2 dB/m, while distances further than 30 m saw an average increased rate of about 0.05 dB/m [31]. This shows that the amount of signal attenuation due to foliage increases steadily with distance until 30 m and then starts to increase at a much slower rate than before, indicating that the distance through foliage does not consistently correlate to the amount of loss. Another experiment completed at 35 GHz showed that when vegetation is close to the transmitter, a greater amount of foliage loss is observed, most likely due to the energy being absorbed. However, less signal attenuation is observed when the location of the foliage is at the midpoint of the transmitter and receiver, most likely because scattering propagates the signal to the receiver [32]. This shows that, although scattering is sometimes seen as an adverse side effect, it can improve signal propagation through vegetation at mmWave frequencies for large enough distances.

Overall, mmWave communications perform best with Line-of-Sight (LOS) between the transmitter and receiver because there are no obstructions, whereas Non-Line-of-Sight (NLOS) relies on multipath to propagate the signal. Building structures in outdoor environments and indoor topologies can cause signal attenuation and energy absorption due to various materials that could obstruct the signal, and can also potentially enable pathways for the signal to be reflected. General research has been completed to test the penetration loss for certain materials at various mmWave frequencies. For indoor environments, drywall was found to have a 6.8 dB penetration loss, as compared to a non-tinted glass with a loss of 3.6 dB at 28 GHz [8]. In indoor environments, the number of obstructions between the transmitter and receiver, rather than distance, is the determining factor for how much loss is attributed to obstructions [8]. A greater number of obstructions means more objects that the signal must move through in order to get to the receiver, which results in the loss of more power. A higher frequency was also shown to increase the amount of penetration

loss that was observed [33]. Some obstructions, such as outdoor building materials, can cause enough loss that the signal does not propagate at all through them [8]. This finding shows that indoor and outdoor mmWave systems may coexist, since they will be completely separated by the outer building structure. Penetration loss does not indicate whether the signal is being reflected or completely absorbed. This is an important distinction to make, because if a signal is being reflected, that could be used to increase the received power when in the right configuration. Studies at 28 GHz and 40 GHz showed that metal, water, and a human hand had similar levels of reflection, but the 40 GHz signal had narrower reflections due to the antenna's smaller beam width [33]. Generally, metal was the best reflector, most likely due to it being a smoother and more uniform surface compared to other materials [14]. Reflection of signals off of surfaces could enable communication via NLOS configurations.

Measurements in the E-band frequency range, which spans from 71 GHz to 76 GHz, are not as prevalent in literature as the lower mmWave frequencies, due to the limited amount of affordable equipment in this range. However, there have been some indoor and outdoor signal propagation measurements completed in this range. Measurements performed in an indoor environment at 72 GHz were consistent with lower mmWave frequency findings, in that the number and type of obstructions dictated the penetration loss, and the number of obstructions contributed to a higher amount of loss [34]. As for reflectivity, the shorter wavelengths caused rough surfaces to create diffuse scattering, making reflection and production of a clear signal more difficult [11]. Outdoor measurements were made at 73 GHz with varying transmitter heights from 7 m to 17 m and transmitter-receiver distances ranging from 30 m to 200 m in the New York City downtown Manhattan area, a dense urban environment. It was found that outages mostly occurred due to NLOS configuration, suggesting that smaller base station units would need to be deployed for this frequency, and indicating the need to depend on multipath signal propagation for NLOS links for successful communication. This is consistent with what was found for lower mmWave frequencies [35].

## 2.2 Functionality of Receiver Hardware Components

In wireless communications, receivers are tasked with sensing and extracting information sent out by transmitters. These signals are also corrupted by noise, which increases the difficulty of interpretation; when noise is particularly severe, simply detecting the signals can become challenging. The focus of this section will be the superheterodyne receiver architecture, which is commonly used to receive radio frequency (RF) signals due to their higher frequencies. The architecture has six major components, as shown in Figure 2.3, namely: RF input, RF amplifier, mixer with local oscillator (LO), intermediate frequency (IF) filter, and IF amplifier [36]. The two main advantages of this type of superheterodyne receiver are its ability to obtain high gain without instability, and the ease with which it can be tuned to different frequencies by changing the frequency of the LO [36]. The main disadvantage for the superheterodyne receiver architecture is the potential for spurious signals to occur. They can occur when the mixer of the receiver is driven into its nonlinear range by an interfering signal, causing cross-modulation on the desired signal at the output of the RF amplifier stage [37]. The following sections will be a high level overview of the different components of the architecture and their functionalities.

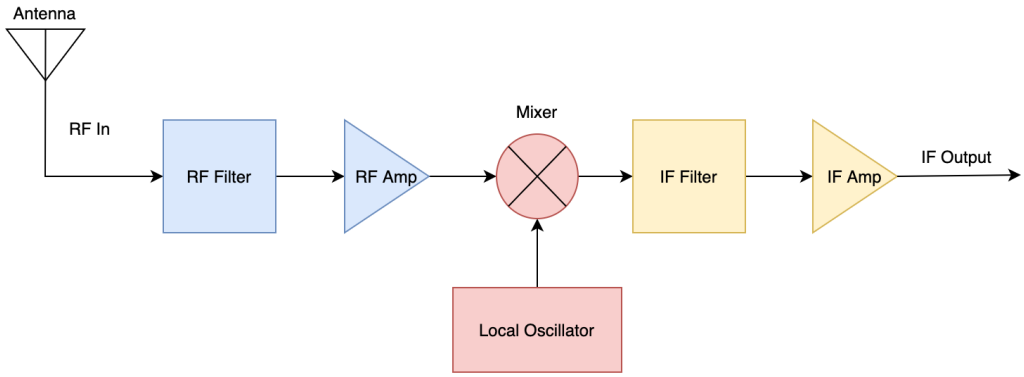


Figure 2.3: When trying to decode signals from a transmitter, a demodulator block is added at the output of the superheterodyne receiver. When simply detecting and sensing the power of signals, this block can be omitted from the block diagram.

### 2.2.1 RF Input and Antennas

The RF input is the point of entrance for the transmitted signal in a receiver. This can be in the form of a wire or, when using wireless communications, an antenna. The main types are wire antennas, aperture antennas, micrcostrip antennas, array antennas, reflector antennas, and lens antennas [38]. The ideal antenna, which would be lossless and have the ability to receive power from all the desired directions, does not exist; as a result, there are many different types of antennas that can be configured to get the desired characteristics for a particular application. In addition to the type of antenna, there are a few key performance metrics that must be considered, including radiation pattern and intensity, gain, polarization, and bandwidth. A radiation pattern is the spatial variation of emitted power from an antenna, since existing antennas are unable to radiate power evenly in all directions [38]. An example of a two dimensional radiation pattern in polar coordinates is shown in Figure 2.4. Radiation intensity is defined as the power per unit solid angle radiated in a particular direction [39]. A major aspect of radiation patterns are the radiation lobes, which are defined as parts of the radiation pattern that are bounded by areas of weak radiation intensity [38]. The major lobe, also called the main beam, contains the direction of maximum radiation; the back lobe is a radiation lobe that is 180 degrees away from the beam of the antenna; and the side lobes are any radiation lobes in directions other than that of the intended main beam [38].

A particularly important antenna parameter, related to radiation lobes, is the half power beamwidth which is the angular width on the major lobe at the points where the signal power is half of its peak value [38]. This can be used to indicate how directional an antenna is, because the half power beamwidth defines where the most signal power is directed; if the width is smaller, then the power of the signal is directed over a smaller area. The gain of an antenna is defined as:

$$G = \frac{P_s}{P_i},$$

where $P_s$ is the maximum radiation intensity from subject the antenna and $P_i$ is the radiation intensity from a lossless isotropic source with the same power input. This provides information about the efficiency of an antenna compared to a hypothetical lossless isotropic

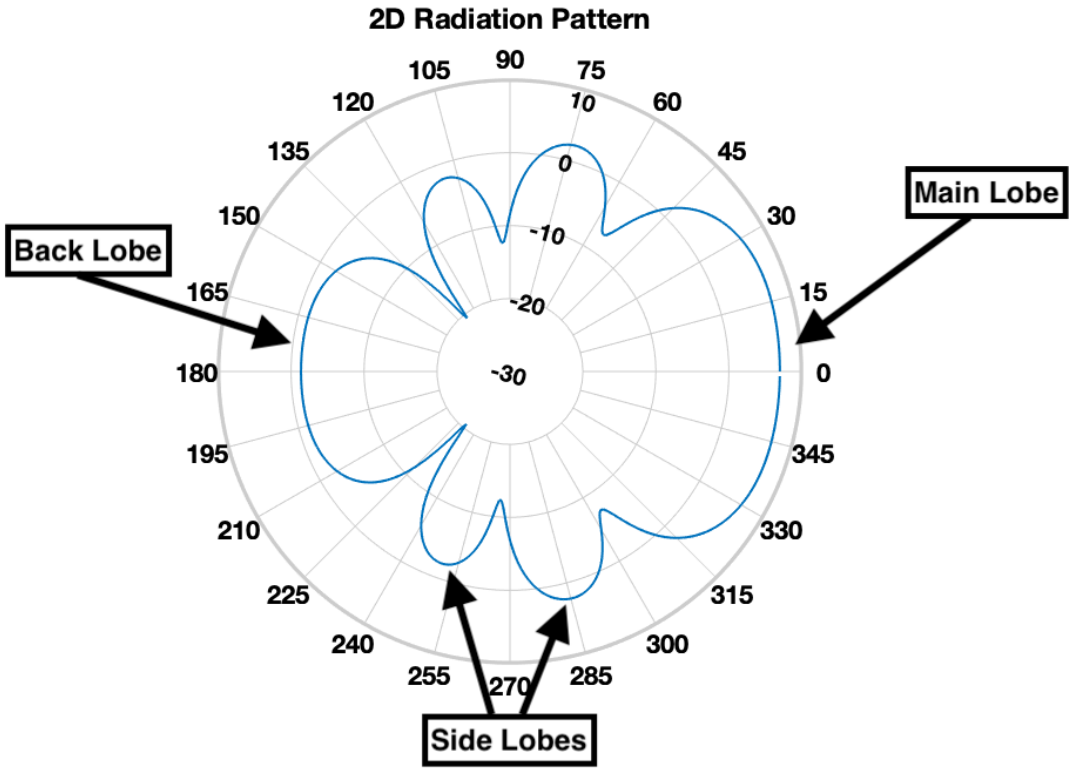


Figure 2.4: This Vivaldi antenna radiation pattern was generated using code from [40] and is an example of the gain and directivity properties at a particular angle.

antenna that can radiate energy equally in all directions [39]. The higher the gain, the stronger the signal an antenna can send or receive in a specified direction. The polarization of an antenna is defined as the direction of the electric field vector [39]. Vertical, horizontal, and circular polarization are shown in Figure 2.5. If the polarization of the antenna does not match the polarization of the radiated wave then a loss of power occurs. Specifically, if they are orthogonal to each other, no power is received; if they are 45 degrees off, the result is a half power loss of the signal [38]. The bandwidth of an antenna is defined as the frequencies at which the antenna is able to operate [38].

Aperture antennas, which are often used for higher frequencies, provide a gradual transition from a waveguide to free space, or vice versa in the case of a receiver antenna [42]. A

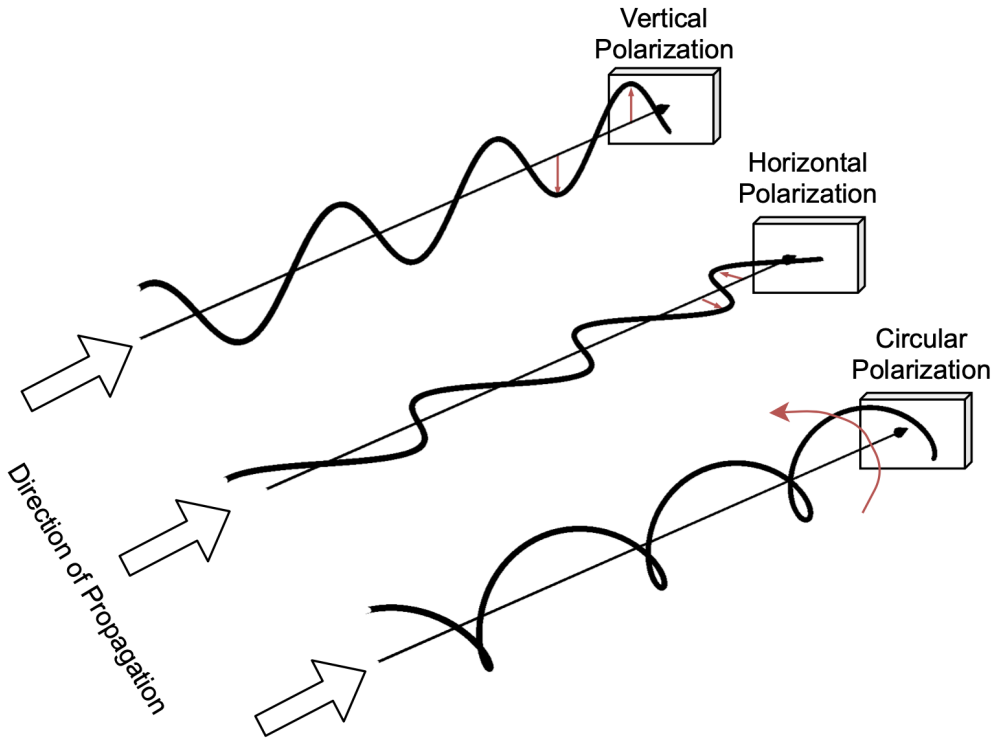


Figure 2.5: Illustrated here are linear polarizations, in the vertical and horizontal directions, and circular polarization. This has been adapted from [41]. Circular polarization occurs when the time-varying signal switches between vertical and horizontal polarization either in a counterclockwise or clockwise direction. The red arrows indicate the direction of the electric field vector for the examples given.

waveguide is a hollow opening that guides the electromagnetic energy along the waveguide in either direction [43]. For mmWave communications, due to high free space path loss and low transmit power, antennas need to have high gain and directivity [44]. A popular choice for mmWave communications are horn antennas, due to their directivity and high gain properties that can be adjusted based on the axial length and aperture of the antenna [42]. The polarization of an antenna is usually defined by the shape of its waveguide [38].

### 2.2.2 Mixer and IF Stage

Once the RF signal has entered the system from the RF input, it is then downconverted to reach the desired IF frequency. This process is completed by a mixer, which essentially takes the product of the input signal and a local oscillator signal. This nonlinear function turns into a signal at a frequency of the difference of the input signal and LO signal,

$$Acos(f_{RF}) * Bcos(f_{LO}) = \frac{AB}{2}[cos(f_{RF} + f_{LO}) + cos(f_{RF} - f_{LO})],$$

since the sum of the two frequencies results in a signal much higher than the desired frequency and can be easily filtered out [37]. The IF frequency can be described in a general formula as:

$$f_{IF} = |f_C - f_{LO}|,$$

where $f_{IF}$ is the intermediate frequency, $f_C$ is the center frequency of the input signal, and $f_{LO}$ is the local oscillator frequency [36]. It is important to note that the mixer linearity only holds if the LO power is high compared to the input signal power [37]. In communications, the reception of unwanted signals, at image frequencies, can occur and cause interference with the desired signal when the signal is downconverted. These signals occur at an image frequency which, for downconversion, can be defined as:

$$f_{IM} = \begin{cases} f_C + 2f_{IF}, & if\ f_{LO} > f_C \\ f_C - 2f_{IF}, & if\ f_{LO} < f_C \end{cases},$$

where $f_{IM}$ is the image frequency and $f_C$ is the center frequency of the RF signal [36]. If $f_C$ is set to 100 kHz and $f_{IF}$ is 50 kHz, then $f_{LO}$ would need to be 150 kHz since 100 kHz + 50 kHz = 150 kHz. If another signal at $f_{IM}$, in this case 200 kHz, is present

at the RF input, then this image signal will be downconverted at the mixer to 200 kHz - 150 kHz = 50 kHz. This causes an issue, since the image signal will now be added to the desired downconverted signal because they are both at the same frequency of 50 kHz. A graphical representation of this example is shown in Figure 2.6. In order to prevent these

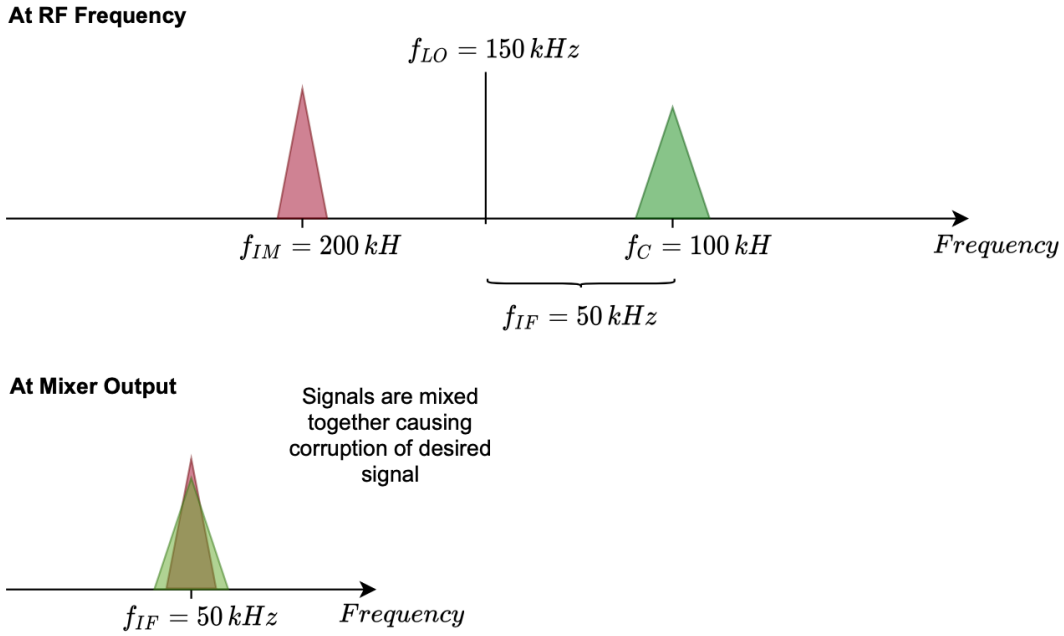


Figure 2.6: A graphical illustration showing how signal corruption can occur if signals at image frequencies are not properly filtered out.

images, a filter before the RF input is necessary. To further remove any spurious responses from other unwanted signals, an IF filter is used [37]. RF and IF amplifiers are also added into the receiver circuit to amplify the desired signal above any possible noise [37].

The LO device provides a steady oscillating signal and often has a variable frequency oscillator, meaning it can be tuned to different frequencies in order to easily change the IF frequency without having to change the entire system to receive different frequencies. Therefore, most frequency synthesizers consist of a voltage-controlled oscillator (VCO) that is incorporated into a feedback control loop, usually in the configuration of a phase-locked loop (PLL) so that the output LO frequency is able to be changed [45]. There are multiple

ways it can be tuned in order to change the frequency, but it is often done via a digital code word sent to the VCO [45]. The code word could be generated from another device such as a microcontroller or computer. There are a few important parameters when choosing the correct frequency synthesizer for an application, including tuning range, minimum step size, and settling time [45]. The tuning range is the range of frequencies that the $f_{LO}$ can be set within. The minimum step size indicates the frequency resolution, meaning the frequency difference between two successive output frequencies. The settling time is the amount of time it takes the system to tune and settle within a frequency window determined by some +/- $f_{ERROR}$ amount [45].

### 2.2.3 Output Signal Modifications

The output after the IF input is not always one signal. Transmitted signals are not usually in the form of a single sinusoidal waveform, but are rather modulated signals whose waveform properties are modified in order to convey information [36]. For example, quadrature amplitude modulation (QAM) transmits information by adding two sinusoidal waveforms whose carriers are 90 degrees out of phase (e.g. sine and cosine) and that are varied in amplitude from each other in order to create unique signals to represent data [18]. Conventionally, the cosine waveform is referred to as the in-phase (I) component and the sine waveform is considered the quadrature (Q) component. After downconversion, depending on the modulation, there could potentially be two output signals that are 90 degrees out of phase. In addition, if the I/Q components are bipolar signals, meaning that they can alternate between negative and positive voltages, then there can also be negative and positive I/Q components, potentially resulting in four signal outputs [36]. If the number of waveforms at the outputs for the received signal is greater than the number of inputs into the final device for data collection, then the outputs can be combined using 180° or 90° hybrid couplers [46]. Hybrid couplers are four port devices that can either split or combine the power of one or several input signals, depending on which ports are utilized [47]. An example of the ports for a 180° hybrid coupler and a 90° hybrid coupler are shown in Figure 2.7. The 180° hybrid coupler operates by inputting either one or two signals into the system. Using the port labels from Figure 2.7, if two signals of equal amplitude and

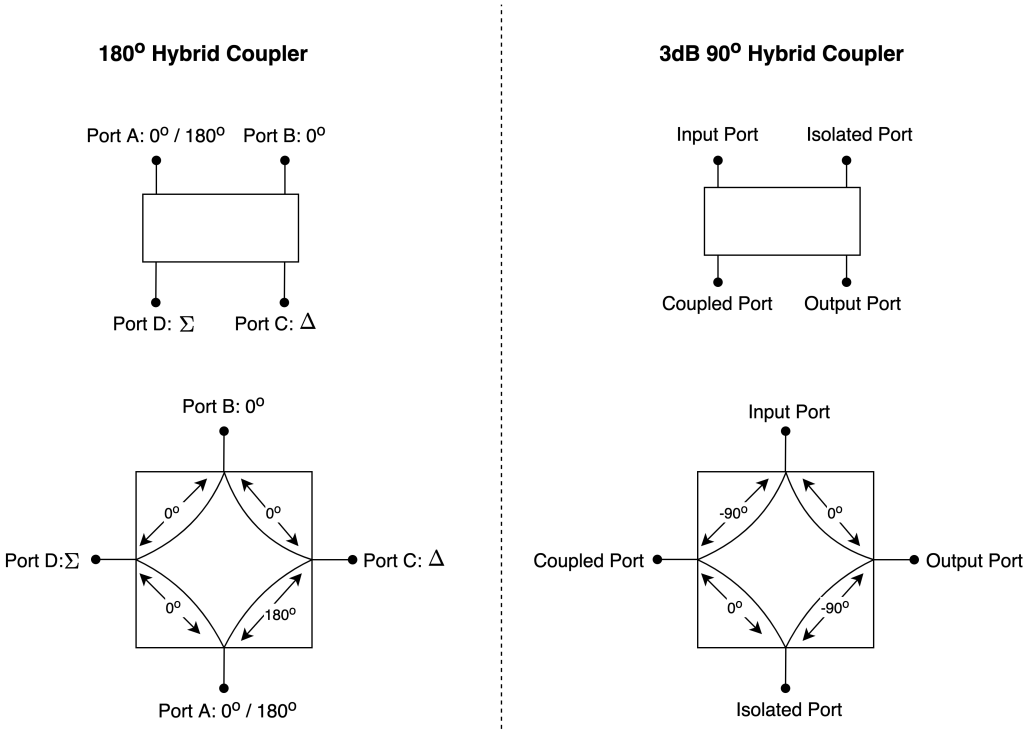


Figure 2.7: An example of possible configurations for a 180 degree hybrid coupler and a 90 degree hybrid coupler which was adapted from [48]. The upper portion of the image shows the port labels and layout while the lower portion shows the phase relationships between the ports.

frequency are applied to port A and port B, then the output at port C would be the vector sum of the signal at port A rotated 180° and the signal at port B, and the output at port D would be the vector sum of the signal at port B and port A [48]. If the two signals of equal amplitude and frequency are also exactly 180 degrees out of phase, then port D would have no power output, as the signals would cancel each other out when added together; in this case, port C would be the sum of the two signals. The opposite would occur if the signals were exactly equal with the same phase. If the coupler only has one input and is utilized as a power splitter, then the output would be two signals of equal amplitude, with the phase being shifted the amount indicated by its path in Figure 2.7 [48].

The 90° hybrid coupler is symmetrical, with the isolated port and input port being rotated by 90 degrees to different outputs. Using the port labels from Figure 2.7, if two signals of equal amplitude and frequency are applied to the input port and the isolated port, then the output port would be the vector sum of the signal at the isolated port rotated by 90 degrees and the signal at the input port, while the coupled port would be the vector sum of the signal at the input port rotated by 90 degrees and the signal at the isolated port [48]. If the two signals of equal amplitude and frequency are also exactly 90° out of phase, then the coupled port and output port values would both be the sum of the isolated port signal and the input port signal. If the 90° coupler is being used as a power splitter, then the output would be two signals of equal amplitude, with the phase being shifted the amount indicated by its path in Figure 2.7 [48].

### 2.2.4 Cables and Storage Considerations

Once the main components of the system have been chosen, the next step is finding the right connectors for each component to join everything together. Some components will be attached via screws and/or dowels, as are waveguide antennas, while other components will have a connector of a specific type, such as SMA, 2.92mm, and N to name a few, and will be of either a male or female gender. This information is provided in the data sheets for each component. A connection can be made as long as both connectors are of the same type and opposite gender. If two connectors are of different types but need to be connected, then adaptors can be used [49]. The components may be connected together, if they are of compatible type or cables can be used. Different types of cables have different operating frequencies that must be taken into consideration when choosing them [49]. Cables can also come in different flexibilities and can be classified by their bendability: rigid, semi-rigid, and flexible. The last major parameter of cables is the amount of power loss that can occur for signals traveling through them. This is usually provided in the data sheets for different frequencies in their operating range.

Once the system with the cables and components has been put together, a link budget analysis can be done to determine the theoretical performance of the system. The link

budget equation calculates the received signal power in dBm:

$$(P_{Rx})_{dBm} = (P_{Tx})_{dBm} + (G_{Tx})_{dBi} + (G_{Rx})_{dBi} - (L_s)_{dB} - (L_a)_{dB},$$

where $P_{Rx}$ is the received signal power, $P_{Tx}$ is the transmit power, $G_{Tx}$ is the transmitter antenna gain, $G_{Rx}$ is the receiver antenna gain, $L_s$ is free space path loss, and $L_a$ is included to account for any additional losses in the system from things such as components or cables [18]. The actual received power strength will most likely be lower than this value due to unknown losses and imperfect components, but the calculated value from the link budget analysis should be approximate. The Signal-to-Noise Ratio (SNR) is another measurement that can be calculated as a check for a receiver system,

$$SNR_{dB} = 10log_{10}\left[\frac{P_S}{P_N}\right],$$

where $P_S$ is signal power and $P_N$ is noise power. Noise can occur from the RF input or generated by components in the receiver system [17].

The hardware for data collection or visualization will be application or research dependent. An analog-to-digital converter (ADC) is used to digitize a signal. In the process of digitization, an analog signal is sampled at a particular sampling frequency which causes the signal to have replicas of itself at intervals of the sampling frequency that can then be filtered out using a low-pass filter [36]. Due to the replicas, the sampling frequency must be two times the bandwidth of the signal according to the Nyquist formula or else the replicas of the signals will interfere with each other causing aliasing and corruption of the signal [17]. Figure 2.8 shows a signal that has been sampled at two times the bandwidth and one that has not, which causes the replicas to interfere with each other. This means that the hardware for data collection must be able to support a sampling rate that is double the maximum bandwidth of the transmitted signal. If the I and Q components are sampled separately with the use of two separate ADCs, then the sampling rate for each must be greater than or equal to the bandwidth of the signal. This still follows the Nyquist formula, as there are still double the amount of samples; they are simply being collected separately, and the individual I and Q samples would need to be combined into their complex signal value for data analysis. The amount of storage space is another requirement that needs to

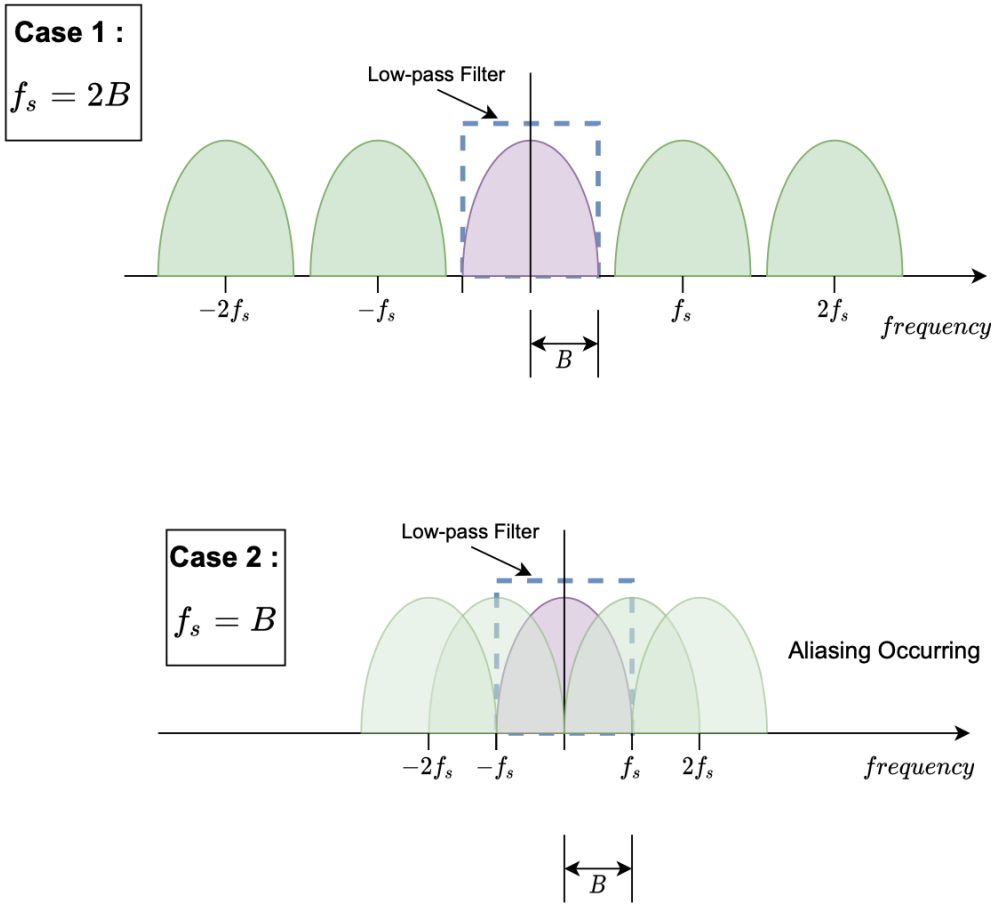


Figure 2.8: An illustration, adapted from [36], of the replicas of a signal when the signal is sampled at two times the bandwidth and when it is sampled at the bandwidth frequency. In the first case, no aliasing occurs and the low-pass filter is able to isolate the desired signal. In the second case, aliasing has occurred and the signal has been corrupted and cannot be recovered.

be taken into consideration. In general the amount of storage necessary is:

$$Storage = D * f_{sample} * b * N,$$

where $D$ is the amount of time it takes to collect one round of data, $f_{sample}$ is the sampling frequency, $b$ is the number of bytes per sample, and $N$ is how many times data will be collected. Let the bandwidth of a signal be 125 MHz, the duration of collection be 10 seconds, the number of collections be 30, and have 4 bytes per sample. The storage needed would be 150 GB; if I and Q components were sampled separately, and each were 4 bytes per sample, the amount of space would be doubled to 300 GB.

## 2.3 Summary

This chapter discussed the physical properties that make mmWave communications more difficult than traditional sub 6 GHz communications, this being due to the small wavelengths of signals in the mmWave frequencies that result in more severe attenuation effects from the atmosphere, weather, buildings, and foliage. It also discussed the superheterodyne receiver architecture and gave a high level overview of the different components in that system. In addition, it provided information about how hybrid couplers operate and how to use them in a design. How to calculate sampling rate and the amount of storage needed was also included in order to bring awareness to potential requirements for hardware used in data collection.

# Chapter 3

# Proposed Custom Framework for Remotely Accessible Outdoor E-band Testbed

The following chapter details the outdoor mmWave portion of the custom testbed. It includes the benefits and drawbacks, given the requirements of the project, that were considered while choosing the hardware that would make the two main communication links. The equipment and layout needed in order to remotely access each radio is also included. This was an important aspect for this particular project because it allowed work to be completed off site, and enabled multiple people to use the hardware for different projects. The physical outdoor setup of the radios and hardware is explained so that it can be easily replicated. The network configuration of the radios that allows data to be easily transferred from one radio to another is detailed. Lastly, alignment issues of the communication link is highlighted.

## 3.1 Commercial Millimeter Wave Radios

The first decision that had to be made was whether to use off-the-shelf radios or build a transmitter and receiver by utilizing downconverters and upconverters along with other

RF hardware components. Table 3.1 shows the radios that were considered and gives the considered pros and cons. The benefits of using commercial radios included the ability to use the radios as they came, and the access to technical support with any issues that could arise. The main benefit for building the radios from individual components was the customization it would allow; it was also potentially less expensive than an all-in-one solution, which could have had more features than were needed. The disadvantages to building a reliable transmitter and receiver were the time and complexity in completing such a task, which could lead to many more potential problems with hardware compatibility, leaving no time to create the signal power detector and make initial out of beam emission measurements. Due to the project's time limit and budget, commercial mmWave radios were the more advantageous option.

Table 3.1: This table lists the main pros and cons of E-band radios that were considered in the selection process.

| Radio | Pros | Cons |
|---|---|---|
| Bridgewave Communications: FLEX4G-1000 | - Familiar with company | - Expensive<br>- 10 Gbps throughput |
| National Instruments: mmWave Transceiver System | - Detailed analysis possible | - Outside budget<br>- Complex System |
| Siklu: EH-1200TX | - Inexpensive<br>- Configurable to 500 Mbps throughput | - Unfamiliar with company |
| Analog Devices: EVAL-ADMV7410 and EVAL-ADMV7310 | - Inexpensive<br>- Customizable system | - Need a lot of additional hardware<br>- Not much technical support for system |

After it was determined that off-the-shelf radios would best meet the needs of the project, different commercial radios were compared based on functionality and cost as shown in Table 3.1. The focus of this project was on E-band, meaning that the commercial radios needed the ability to operate in the frequencies ranging from 71-76 GHz. Many mmWave radios on the market, especially those in E-band, are advertised to customers as low latency backhaul solutions. Backhaul communication lines are high capacity links, meaning they have high bandwidths and data rates. As a result, many of the radios had data rates up to 10 Gbps, which was more than what was necessary for the project. Many of the radios also worked at great distances; since these projects would be set up at a distance of less than a mile, the radios needed to be able to operate at shorter distances. Another

major requirement for these radios was the ability to tolerate outdoor weather, as these radios would be staying outside. The last requirement was the ability to remotely log into and configure the radios so that onsite presence would not be necessary. Therefore, the ideal radio was a relatively inexpensive one that would not have an excessive amount of unnecessary software features.

The commercial radios ultimately chosen were the Siklu Etherhaul 1200TX radios with a 1-foot antenna, as shown in Figure 3.1. Close up images of the antenna, side, and back of a radio are shown in Figures 3.2, 3.3, and 3.4 respectively. These radios are transceivers that operate in the necessary frequency range of 71-76 GHz and have a data throughput of up to 500 Mbps. Since each radio can both transmit and receive, they utilize time division duplexing (TDD) to allocate different time slots for the uplink and downlink in order to operate at the same frequency and not interfere with each other. Transmission Control Protocol (TCP) is the standard they used to transfer data, indicating that data was sent via packets. The bandwidth of the radios can be configured to 125 MHz, 250 MHz, or 500 MHz, and can also change the data throughput. FCC licenses were purchased through Siklu, and the two communication links were registered in order to ensure the legality of any experiments completed. The radios were built for outdoor use; this means that they are weatherproof, which allowed them to be kept outdoors once they are completely set up. The operating temperature range of the radios is -45°C to 55°C, which was important since they would need to stay outside for the majority of the summer and winter in Massachusetts. The radios also had Power over Ethernet (PoE) capabilities, meaning that additional power cables would not be needed. Remote access to the radios was possible either through a web-based system or a command line interface where connection was established through secure shell protocol (SSH).

## 3.2 Remote Access to Radios

Each of the radios needed to be connected to a server in order for them to be operated. It was decided that three servers, running Ubuntu 20.04, would be used for the four radios. One server had both Radio B and Radio C connected to it and would act as a transitional


Figure 3.1: Four of these commercial radios were used to create two separate communication links, as it would create extra work to turn the middle radio and have to realign the radios each time. This configuration also allows a seamless data transmission through the two data links.

Figure 3.2: An image of the 1 ft Siklu Antenna. The specific part number is: 73-EH-ANT-1FT-B.

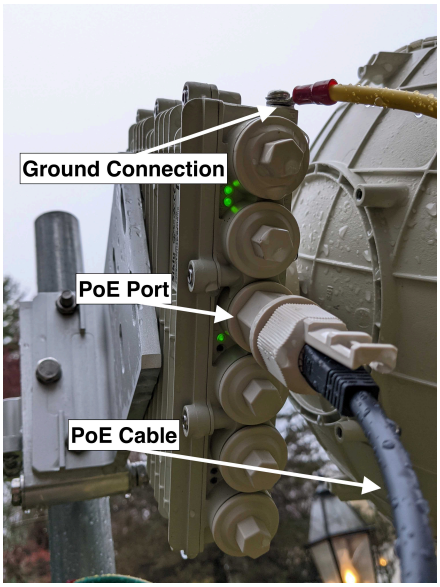


Figure 3.3: A side view of the Siklu radio. The yellow wire is the ground connection and the black wire is the PoE connection.


Figure 3.4: A picture of the back of the Siklu radio mounted on a non-penetrating roof mount and approximately 7 feet in the air.

node from the first link to the next link. The radios and outdoor setup were at a private home residence, so security was a concern when trying to determine the best method to allow remote access. One option that was initially considered was to utilize port forwarding on the servers. This would enable other computers outside the home network to be able to access the server; however, this created security risks, as there was no way to ensure that unwanted users would not attempt to access the network through the open port. The solution to this security issue was to use a radio access point (RAP) that also had a hardware virtual private network (VPN). This hardware was was obtained through Worcester Polytechnic Institute. It allowed the servers to appear as though they were a part of the school's network and create a secure encapsulated and encrypted tunnel for data to travel through, keeping the home network safe from potential attacks. The remote access network configuration is shown in Figure 3.5.

The network setup allowed a user, who had logged into a software VPN provided by WPI, to use these servers. There was no graphical user interface nor monitor attached to these servers, so secure shell protocol (SSH) was used to log into the computers to establish

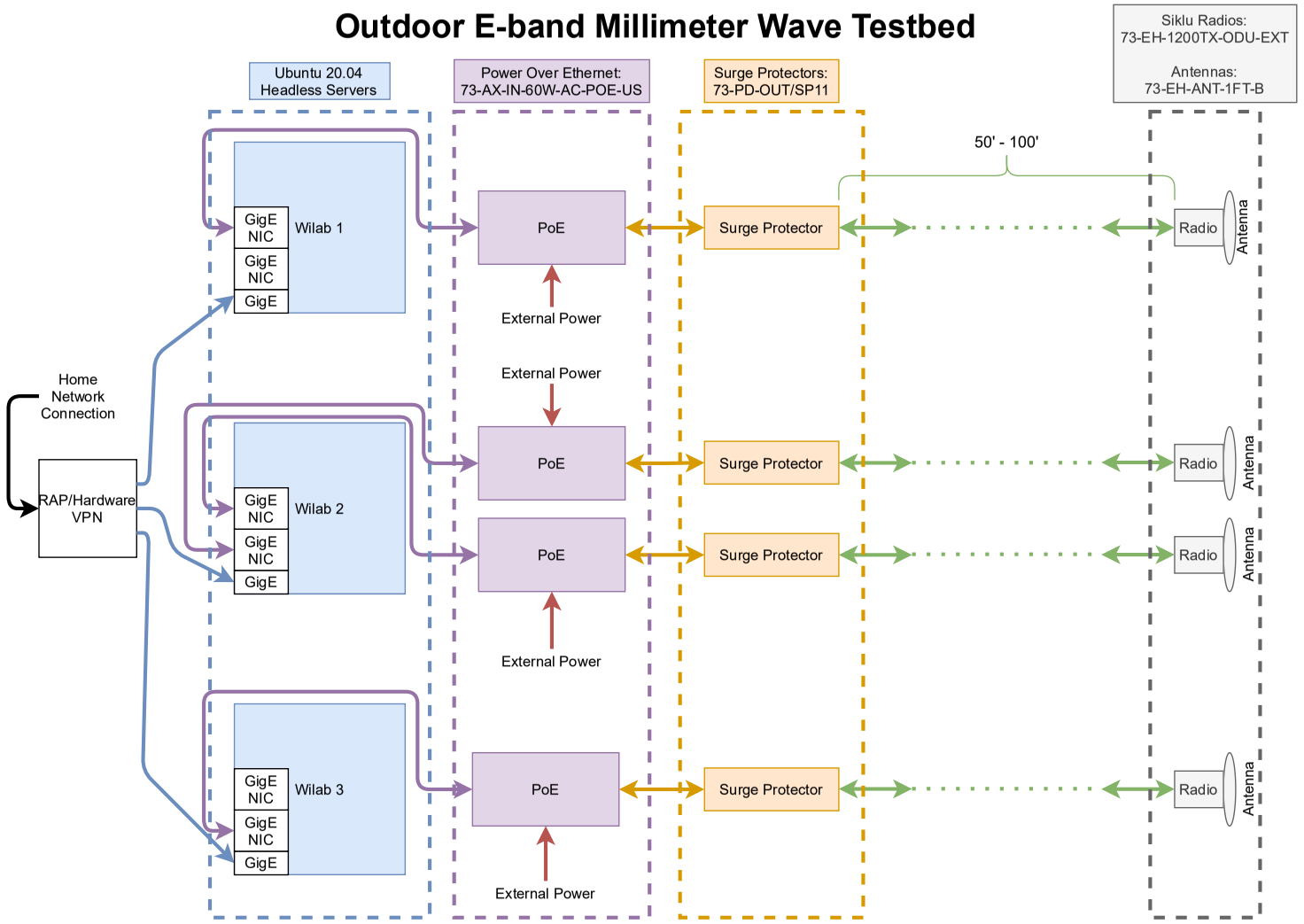




Figure 3.5: The RAP/hardware VPN, and servers were inside the house. GigE shielded cables were connected to the Siklu Radios beside the house.

a secure remote connection. The main reason for not using a monitor was ease of use, since SSH connection can be established using available software such as PuTTY or by using the terminal command:

```
ssh username@IP_ADDRRESS
```

which prompts the user to input a password for added security. A unique username and password was created for each individual who needed to access the server in order to forgo the need to share password information. The lack of a GUI meant that the radios would need to be controlled via the command line interface (CLI). The username, internet protocol (IP) address, and password to access the radios could be changed but were constant for each user that had access on the server.

## 3.3 Physical Setup of Radios

The first step in the physical setup of the radios was to attach them to non-penetrating roof mounts that stood approximately 8 ft tall with the radios attached around 7 ft from the ground. A conceptual diagram of the radio configuration is shown in Figure 3.6 and an image of the actual setup is provided in Figure 3.7.

Each of the three roof mounts represents a node, with Radio A and Radio D attached to Node 1 and Node 3, respectively. Node 2 had both Radio B and C attached to it, with Radio C positioned slightly higher on the roof mount in order to accommodate both radios being on the same node. Pictures of the three nodes are shown in Figure 3.8. All four radios were grounded via a wired connection to a grounding rod that was buried at each node to ensure proper grounding in case one of the radios was to be struck by lightning. Radios operating in millimeter wave frequencies need to be aligned carefully because of the small beamwidth of the antennas. The ground that the radios were on was grass and dirt, which could have caused misalignment since frost and rain can cause the ground to shift around. To prevent this from happening, the radios were placed on a layer of gravel so that any liquid could drain and not affect the alignment. Large rocks were put onto the roof mounts to ensure that they would not be moved by wind.

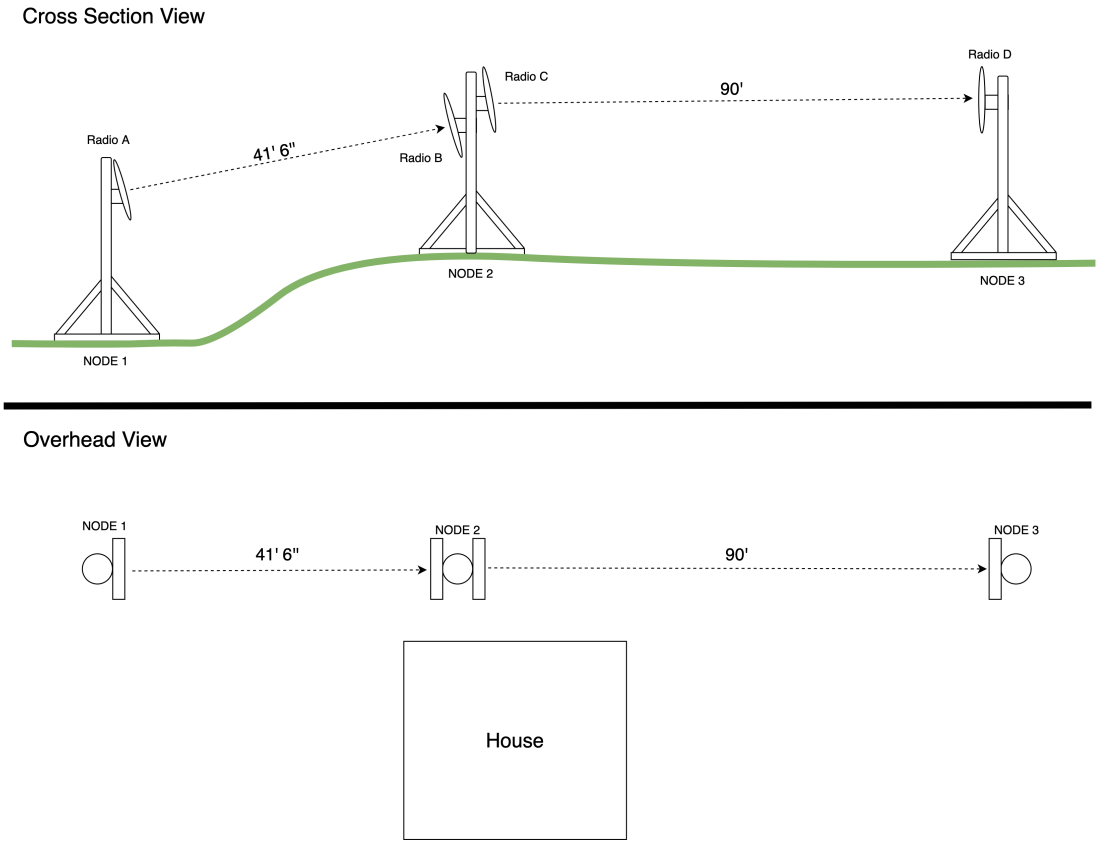


Figure 3.6: Node 1 was slightly below Node 2; the angle between them was approximately 10°. The angle between Radio C and Radio C was approximately 6°.


Figure 3.7: This image was taken in a panoramic style, causing the radios to appear as if they were in a curved formation; however, they are in a straight line-of-sight configuration.

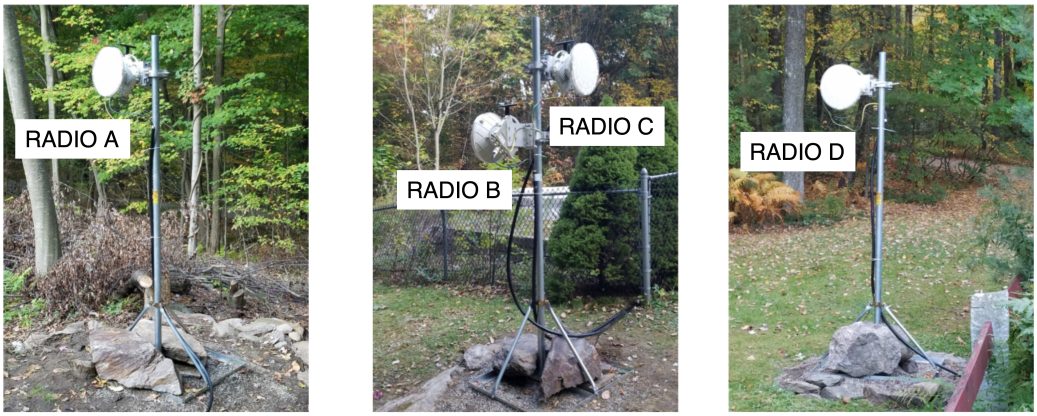


Figure 3.8: Radio A and Radio B made up one communication link that was around 41 ft and 6 in apart. Radio C and Radio D made another communication link that was approximately 90 ft apart.

Each radio had two connections: a shielded 50-100 ft CAT6 cable as well as a wire connecting to the grounding rod. The gigabit Ethernet (GigE) cables, for all four radios, were put into a thick plastic weatherproof hose and then buried underground for safety. The hose led into a basement window that was covered except for four holes for the GigE cables. A surge protector for each GigE connection was used for safety, as shown in Figure 3.9; if

a lighting strike or an excessive amount of current suddenly came in through the lines, the surge protector would redirect the energy so that it would not go through the line to the servers. The GigE cables were then connected to PoE injectors, which were then connected to power and to the servers for each radio as shown in Figure 3.10. The PoE injector then

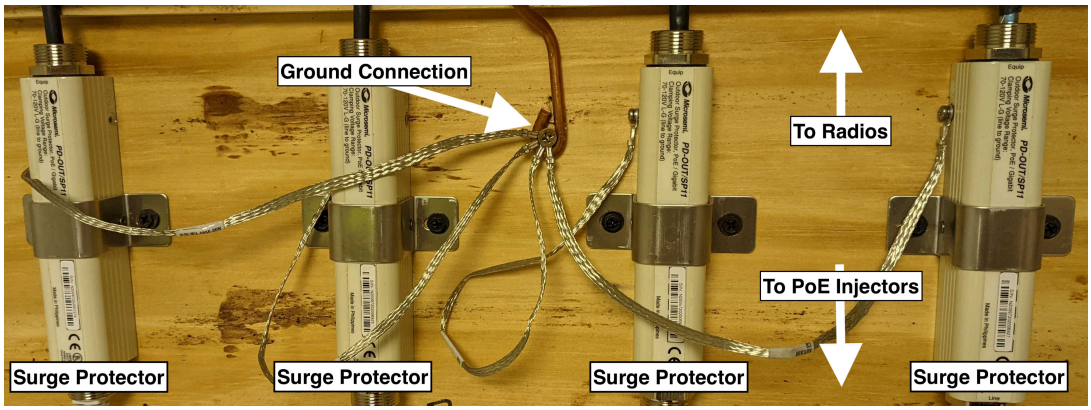


Figure 3.9: An image of the four surge protectors that connected each GigE cable from its respective radio to its PoE injectors.

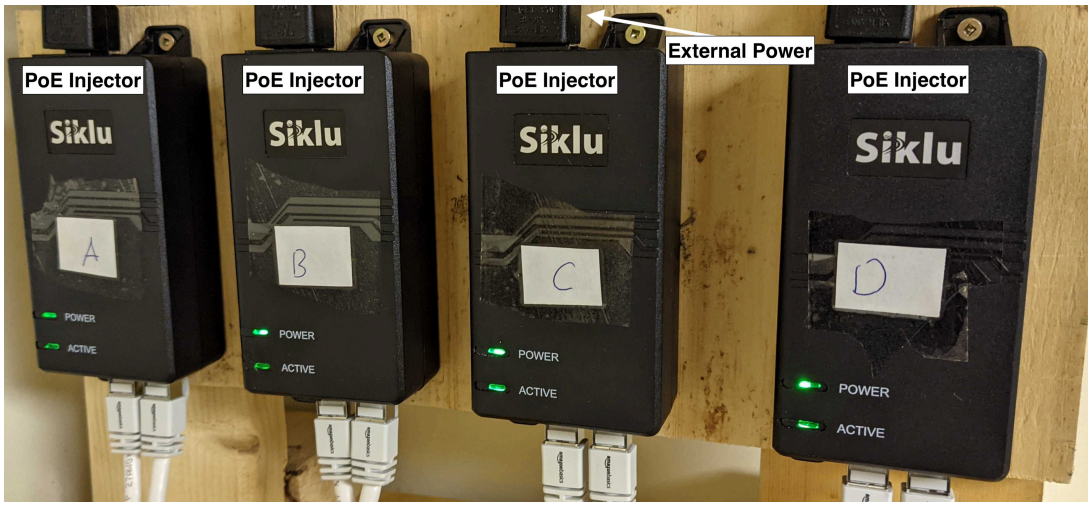


Figure 3.10: An image of the four PoE injectors that had a GigE connection to each radio's respective server and a connection to an 120V external power plug.

had a cable that was connected to a GigE network interface card (NIC) that was connected

to the server. This enabled data to travel between the server and radio.

## 3.4 Network Configuration of the Radios

Once the physical setup was complete, the next step was to ensure that the radios and servers could be easily accessed. Initially, each radio and its network interface on the server had the same local IP address; however, this created issues because all the servers were connected and communicating via the RAP. When attempts were made to access a specific radio on the server that it was connected to, an issue would occur where a different radio than the desired one would be accessed. This was solved by putting each radio and its network interface, onto different sub networks from the other radios, as shown in Figure 3.11. The first step in setting up this configuration was reassigning IP addresses to each radio.

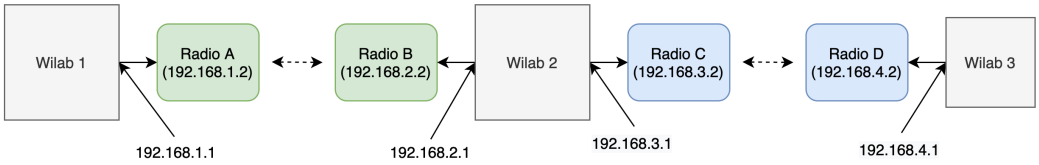


Figure 3.11: A diagram showing the IP address setup. The server Ethernet ports all had IP addresses that ended in ".1" and the radio IP addresses ended in ".2" to better organize the network.

This was completed via the CLI command:

```
set ip 1 ip-addr static IP_ADDRESS prefix-len 24 vlan 0
```

which changed the main IP address for each radio. The next step was to change the IP address of each network interface. This was completed by first seeing which network interface the radio was connected to. Then by using the command:

```
sudo ifconfig INTERFACE_NAME  IP_ADDRESS
```

the network interface IP address could be changed.

Once the IP addresses were set up correctly, the next step was to configure the network to allow data to be sent from the server connected to Radio A to the server connected to Radio D. This was accomplished via IP routing, as shown in the following example command:

```
ip route add 192.168.2.0/24 via 192.168.1.1
```

which tells the server that all packets with a destination address from 192.168.2.0 to 192.168.2.255 should go out through the network interface 192.168.1.1. This command was then repeated two more times:

```
ip route add 192.168.3.0/24 via 192.168.1.1
ip route add 192.168.4.0/24 via 192.168.1.1
```

to ensure that any packets that needed to go through the network would be going through the right network interface. This was repeated for each interface to ensure data could be freely transferred between the servers.

Two methods were used to transfer information in order to verify that the radios were communicating. The first method was transferring a file from each server. This was accomplished through the following command:

```
scp -o BindAddress=192.168.1.1 FILE_NAME ymbrown@192.168.2.1
```

which uses secure copy protocol (SCP) to send a file through the radio network interface, in this case Radio A, and prompts the user for their password to transfer the file. Figure 3.12 and Figure 3.13 show an example of a successful file transfer from Wilab1 to Wilab2. It could then be repeated,

```
scp -o BindAddress=192.168.3.1 FILE_NAME ymbrown@192.168.4.1:
```

to transfer the file from the Wilab2 to the final server destination of Wilab 3.

The last method to get consistent data transfer between the radio links, meaning between Radio A and Radio B or Radio C and Radio D, is to use iPerf, which is a tool that can produce standardized performance measurements for networks. Specifically, iPerf3 was utilized. The type of data being transferred between the radios for out-of-beam emission measurements does not matter, so long that it is standard and repeatable, which iPerf can

```
[ymbrown@wilab1:~$ ls
 answerbot       questions   sshlog_2020_13_09_02_10.txt  ymbrown@192.168.2.1
 F027398593.lic  script.exp  sshlog_test.txt
 log_file        siklu       test
[ymbrown@wilab1:~$ touch example_file.txt
[ymbrown@wilab1:~$ ls
 answerbot         log_file    siklu                        test
 example_file.txt  questions   sshlog_2020_13_09_02_10.txt  ymbrown@192.168.2.1
 F027398593.lic    script.exp  sshlog_test.txt
[ymbrown@wilab1:~$ scp -o BindAddress=192.168.1.1 example_file.txt ymbrown@192.168.2.1:
 ymbrown@192.168.2.1's password:
[example_file.txt                              100%    0     0.0KB/s   00:00
```

Figure 3.12: Wilab1 terminal where a file called example_file.txt was created and then sent to Wilab2 via the SCP command. This file traveled from the server through Radio A's network interface to Radio A to Radio B and then to Wilab2.

```
[ymbrown@wilab2:~$ ls
 F027398582.lic  F027398584.lic  test  uploaded_files
[ymbrown@wilab2:~$ ls
 example_file.txt  F027398582.lic  F027398584.lic  test  uploaded_files
 ymbrown@wilab2:~$
```

Figure 3.13: Wilab2 terminal which showed the original files on the server before the file transfer from Wilab1. When the files were looked at again after the file transfer, the example_file.txt was shown to have been successfully transferred.

accomplish. To use iPerf between Radio A and Radio B, the following command could be used to make Wilab1 the server:

```
iperf3 -s -B 192.168.1.1
```

Then, this command could be used:

```
iperf3 -c 192.168.2.1
```

to make Wilab2 the client. The default time is 10 seconds, but that could be changed by adding `-t TIME_IN_SECONDS` onto the client command. An example of iperf in use is shown in Figure 3.14 for server setup and Figure 3.15 for client set up. Figure 3.16 plots the data throughput versus time for one iPerf test over a 10 second interval. The bandwidth of the radios was set to 125 MHz, therefore a bit-rate of approximately 111 Mbits/s shows that

it was using almost the full bandwidth. The adaptive modulation was turned off for the radios and instead was set to qam64. When adaptive modulation was turned on the bitrate was lower since the radio would change the modulation, and thus the amount of data that could travel through the link, based on its quality of link readings.

```
ymbrown@wilab1:~$ iperf3 -s -B 192.168.1.1
-----------------------------------------------------------
Server listening on 5201
-----------------------------------------------------------
Accepted connection from 192.168.2.1, port 35634
[  5] local 192.168.1.1 port 5201 connected to 192.168.2.1 port 35636
[ ID] Interval           Transfer     Bitrate
[  5]   0.00-1.00   sec  13.2 MBytes   110 Mbits/sec
[  5]   1.00-2.00   sec  13.2 MBytes   111 Mbits/sec
[  5]   2.00-3.00   sec  13.2 MBytes   111 Mbits/sec
[  5]   3.00-4.00   sec  13.2 MBytes   111 Mbits/sec
[  5]   4.00-5.00   sec  13.2 MBytes   111 Mbits/sec
[  5]   5.00-6.00   sec  13.2 MBytes   111 Mbits/sec
[  5]   6.00-7.00   sec  13.2 MBytes   111 Mbits/sec
[  5]   7.00-8.00   sec  13.2 MBytes   111 Mbits/sec
[  5]   8.00-9.00   sec  13.2 MBytes   111 Mbits/sec
[  5]   9.00-10.00  sec  13.2 MBytes   111 Mbits/sec
[  5]  10.00-10.01  sec  65.0 KBytes   104 Mbits/sec
- - - - - - - - - - - - - - - - - - - - - - - - -
[ ID] Interval           Transfer     Bitrate
[  5]   0.00-10.01  sec   132 MBytes   111 Mbits/sec                  receiver
-----------------------------------------------------------
Server listening on 5201
-----------------------------------------------------------
```

Figure 3.14: Wilab1 was initialized as the server and then connected to Wilab2, as shown by the "Accepted connection from 192.168.2.1" message. This then gave information about the transfer speed and bitrate for each one second time interval. The bandwidth was set to 125 MHz for this test, so a bitrate of 110 Mbps is expected.

## 3.5 Radio Alignment

The received signal strength of the radios were measured and compared to values obtained from a link budget analysis in order to determine how well the system was performing. The communication link from Radio A to Radio B and the link from Radio C to Radio D were tested. The radios had a spectrum analyzer functionality, which could be used via this command:

```
spectrum-analyzer start FREQUENCY-BANDWIDTH
```

where the frequency could span a range or be a specific value, and the bandwidth could be

```
ymbrown@wilab2:~$ iperf3 -c 192.168.1.1
Connecting to host 192.168.1.1, port 5201
[  5] local 192.168.2.1 port 35636 connected to 192.168.1.1 port 5201
[ ID] Interval           Transfer     Bitrate         Retr  Cwnd
[  5]   0.00-1.00   sec  13.6 MBytes   114 Mbits/sec   10   70.7 KBytes
[  5]   1.00-2.00   sec  13.2 MBytes   111 Mbits/sec   11   70.7 KBytes
[  5]   2.00-3.00   sec  13.1 MBytes   110 Mbits/sec    9   76.4 KBytes
[  5]   3.00-4.00   sec  13.2 MBytes   111 Mbits/sec   10   70.7 KBytes
[  5]   4.00-5.00   sec  13.2 MBytes   111 Mbits/sec   11   72.1 KBytes
[  5]   5.00-6.00   sec  13.2 MBytes   111 Mbits/sec    7   72.1 KBytes
[  5]   6.00-7.00   sec  13.2 MBytes   111 Mbits/sec   10   76.4 KBytes
[  5]   7.00-8.00   sec  13.2 MBytes   111 Mbits/sec    9   69.3 KBytes
[  5]   8.00-9.00   sec  13.2 MBytes   111 Mbits/sec    8   70.7 KBytes
[  5]   9.00-10.00  sec  13.1 MBytes   110 Mbits/sec    9   70.7 KBytes
- - - - - - - - - - - - - - - - - - - - - - - - -
[ ID] Interval           Transfer     Bitrate         Retr
[  5]   0.00-10.00  sec   132 MBytes   111 Mbits/sec   94             sender
[  5]   0.00-10.01  sec   132 MBytes   111 Mbits/sec                  receiver

iperf Done.
ymbrown@wilab2:~$
```

Figure 3.15: Wilab2 was initialized as the client and then connected to Wilab2, as shown by the "Connecting to host 192.168.1.1..." message. It then gave information about the transfer speed, bitrate, number of retransmitted packets, and congestion window for each one second time interval.

set to 125 MHz, 250 MHz, or 500 MHz. This would then output a received signal strength (RSS) value. A theoretical link budget analysis was completed for both communications links. The Radio A to Radio B communication link was set to 74.375 GHz with a 500 MHz bandwidth, and the distance of the link was 41.5 ft. The Radio C to Radio D communication link was set to 73.875 GHz with a 500 MHz bandwidth, and the distance of the link was 91 ft. The gain of all the Siklu antennas was 43 dBi. The transmit power was varied from -35 dBm to -10 dBm for the link from Radio A to Radio B, as a transmit power greater than -10 dBm could have potentially caused damage to the receiver radio due to their close distance. The transmit power was varied from -35 dBm to 0 dBm for the link from Radio C to Radio D; due to the greater distance between these radios, damage to the receiver radio was not a concern. Figure 3.17 shows the comparison of the theoretical RSS, calculated with the link budget equation, to the measured RSS values. The measured RSS values are about 20 dBm lower than the theoretical values. This discrepancy can be attributed to a misalignment of the antennas. The antennas on the radios had a half power beamwidth of 0.9°; this means that if the antennas were off center by just 0.9°, half of the transmit power would have been lost. This result was expected, since there was some difficulty in

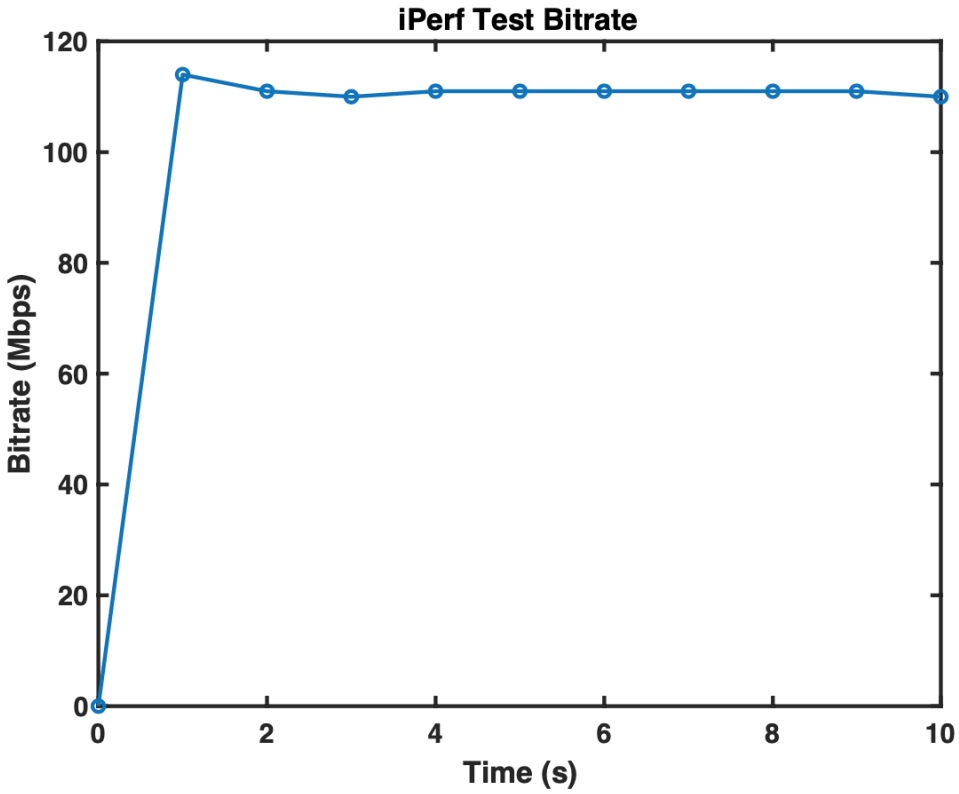


Figure 3.16: A graph showing the bitrate over time for one iPerf test. The bitrate is shown to reach a steady peak of around 111 Mbps which is within normal range for a bandwidth of 125 MHz.

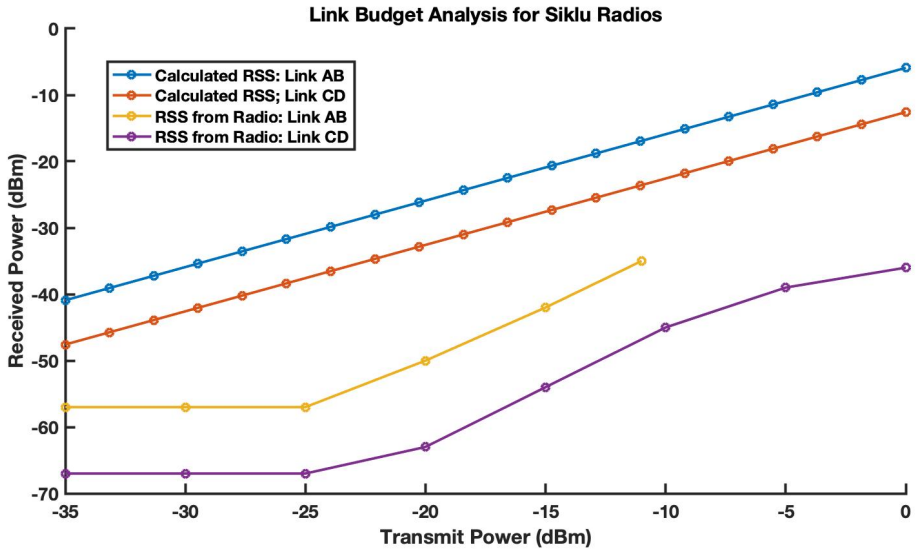


Figure 3.17: A graph comparing the theoretical received power to the measured received power. There is about a 20 dBm difference for both radio links indicating that the antennas were not perfectly aligned.

aligning the antennas. When in alignment mode, the antennas did not produce consistent values while they were being adjusted, which would have indicated that they were properly aligned. Instead, the values varied greatly,which made this task difficult.

## 3.6 Summary

This chapter covered the decision process for choosing the 1200TX Siklu radios as the commercial radios used to create the two communication links. Remote access to all the servers was accomplished through a RAP/hardware VPN, while maintaining security for the home network that this testbed resided in. The physical setup of the radios was also included. However, the roof mounts and PoE setup depended on the type of equipment and could change drastically. The last section focused on configuring the network. Four subnets, one for each radio, were created to avoid confusion. IP routing was completed in order to be able to direct packets with destinations to different radios through the appropriate network

interface. The two methods to send data, SCP and iPerf, were explained, and examples for both were shown. The issue of antenna alignment causing lower than expected received signal strength of the radios was mentioned.

# Chapter 4

# Custom-Built Millimeter Wave Measurement Platform

This chapter presents details regarding the creation of the custom-built measurement platform. The main purpose of the system was to detect and visualize power levels of received signals with an Agilent CSA N1996A Spectrum Analyzer. Figure 4.1 shows a basic diagram of the receiver system. The antenna would need to be 7 ft from the ground to detect signals from a Siklu radio and so the downconverter component would have to be relatively light. The downconverter also needed to be able to output signals at or below 3 GHz, due to that being the frequency limit of the spectrum analyzer. The component selection process is outlined, along with technical details about the final components. A link budget analysis is included to provide insight into the theoretical performance of the system. The overall structures and connections are also detailed to show how the individual components fit together. Lastly, information about the enclosures that were built for this system is included.

## 4.1 Component Information

The first component that needed to be chosen was the downconverter, as the whole system would be built around this requirement. The downconverter also needed to be an

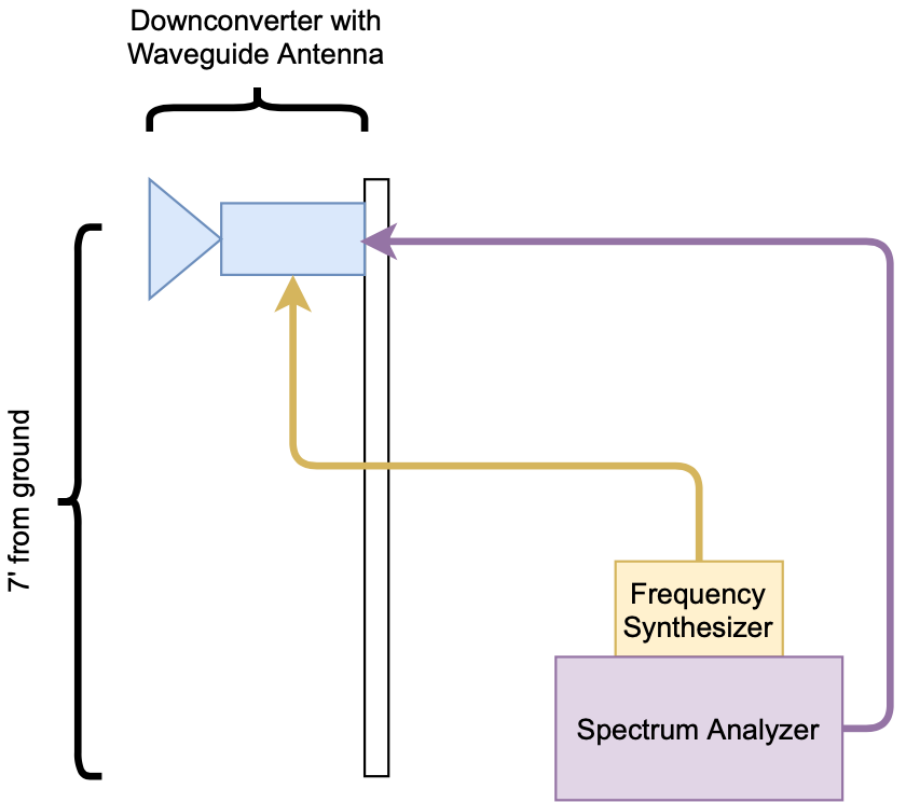


Figure 4.1: A simple diagram showing the major components for the receiver system which includes a spectrum analyzer for visualization of the signal and a frequency synthesizer as an LO driver for the downconverter.

evaluation board or a package system to avoid the need to create a circuit for the system, which would not have been possible due to time constraints. The main considerations while choosing this component were the operating frequency range, bandwidth, IF frequency range, and the RF input type. The operating frequency range needed to cover the whole E-band, which spans 71-76 GHz, as that is the range for the commercial Siklu radios of the outdoor testbed. The RF input type had to have some sort of attachable antenna to ensure that wireless signals could be received. The bandwidth had to be able to cover the maximum bandwidth of 500 MHz of the siklu radios. The IF frequency range needed to be

Table 4.1: A table that compares the different downconverter/spectrum analyzer choices and includes the main pros and cons that were considered.

| Downconverter/<br>Spectrum Analyzer | Pros | Cons |
|---|---|---|
| SAF Tehnika: Spectrum Compact | - All in one solution<br>- Remotely accessible<br>- Small, handheld<br>- powered via one cable | - Expensive<br>- Unknown company<br>- no I/Q samples |
| Analog Devices: EVAL-ADMV7410 | - inexpensive<br>- Outputs I/Q<br>- small<br>- well known company | - Need to find additional hardware (power supply, couplers, LO input)<br>- not much technical support |
| Eravant: E-band Down-converter | - Extended frequency range 60 GHz - 90 GHz | - Expensive<br>- LO range: 10 GHz to 15 GHz<br>- large |
| Keysight Technologies: Field Fox | - All in one solution<br>- Small, handheld<br>- Remotely accessible<br>- Well known company | - Expensive<br>- More features than needed<br>- Additional hardware needed to extend frequency<br>- No I/Q samples |

close to baseband to ensure it could work correctly with the final device that would collect data. Table 4.1 shows the final downconverters that were considered and lists the major pros and cons of each of them.

The downconverter that was chosen was the Analog Devices EVAL-ADMV7410 evaluation board [50], shown in Figure 4.2. This downconverter operates in the E-band frequency with an RF input on the back of the board that interfaces with a waveguide WR-12 antenna. An external +/- 5 V is used to power the downconverter. This downconverter has an 2 GHz bandwidth and an IF frequency range of 2 GHz to baseband, meaning that it would be well within the bandwidth and frequency requirements after downconversion for the spectrum analyzer. The LO input requires a signal from 11.5 GHz to 13 GHz to be able to down convert the signal from 71 GHz to 76 GHz to 2 GHz to baseband. These requirements exist because the downconverter is driven by a 6x LO multiplier. The result of this multiplier is a modification to the formula to calculate IF frequency,

$$f_{IF} = f_{RF} - 6f_{LO},$$

where the LO frequency is multiplied by six.

The power supply used for the downconverter had to satisfy the power requirement of

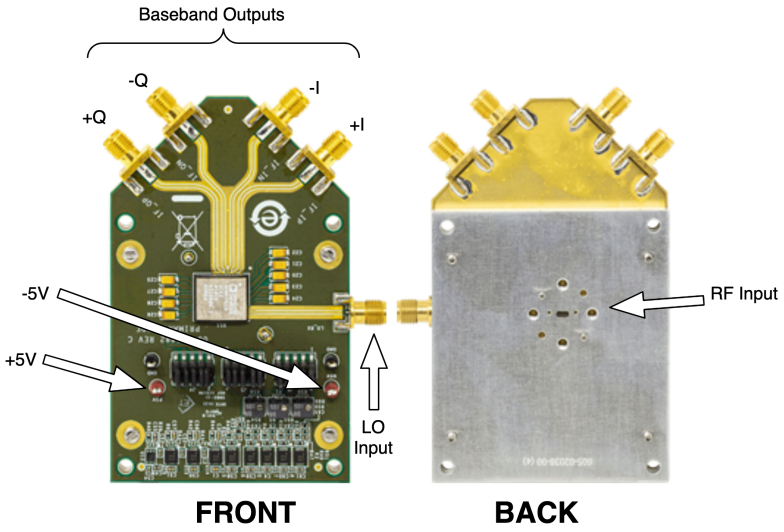


Figure 4.2: A picture of the AMDV7410 evaluation board from [51]. It uses the fully integrated system in package AMDV7410 low noise E-band downconverter from Analog Devices. Data sheets for the AMDV7410 and its evaluation board can be found at [52] and [50] respectively.

+5 V and -5 V. The current requirement was calculated by looking at the data sheet to see the maximum power dissipation rating, which was found to be 1.25 W. Using the equation,

$$P = IV \rightarrow \frac{P}{V} = I = \frac{1.25W}{5V} = 0.25\,A,$$

the current requirement was found to be 250 mA. In addition to the voltage and current constraints, the downconverter board also had a specified start up sequence that had to be followed in order to prevent damage to the board. First the -5 V power supply had to be turned on, followed by the 5 V power supply. Next, Pin 1 & 2, on the board had to be connected. The last step was to turn on the LO input. The solution was to use two 5 V power supplies and configure them in a way to act as a dual power supply. The chosen components were two of the RS-15-5 5 V power supplies from Mean Well, as shown in Figure 4.6.

Once the downconverter was finalized, the next components that needed to be chosen

were two 180° hybrid couplers and one 90° hybrid coupler, which would join the four baseband outputs of the downconverter into one output. The chosen 180° hybrid coupler was the ZAPDJ-2-S+ from Mini Circuits [53], shown in Figure 4.3. They operate from

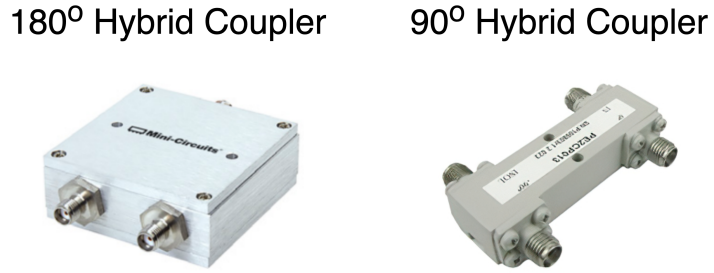


Figure 4.3: The 180° and 90v hybrid couplers used to combine the downconverter outputs into one single output. The 180° hybrid coupler shown is from [53] and the 90° coupler is from [54].

1 GHz to 2 GHz, meaning that the maximum possible bandwidth of the Siklu radios of 500 MHz would be usable; however, it would further limit the IF frequency to 1 GHz to 2 GHz, rather than from baseband to 2 GHz. The chosen 90° hybrid coupler was the PE2CP013 from Pasternack [54], shown in Figure 4.3, which also operates from 1 GHz to 2 GHz. The impedance of these components were also both matched to be 50 Ohms in order to limit the loss of power as the signal travels through them.

The next major component to be chosen was the WR-12 antenna. The gain of the antenna needed to be high, as millimeter wave signals are heavily attenuated in free space. WR-12 antennas are standardized for use in the 60-90 GHz range, so the 261E-25/387 Mi-Wave E-band antenna was chosen [55]. It is a pyramidal horn antenna with a 25 dBi gain, shown in Figure 4.4. It is linearly polarized and has a 3 dB beamwidth of 9° and 10° for vertical and horizontal polarization, respectively. The last component to be chosen was the LO input, which needed to be able to operate in the frequency range of 11.5 GHz to 13 GHz. The most difficult aspect of choosing this equipment was finding one that was low in cost. The final product was the MLSP1113 frequency synthesizer from Micro Lambda Wireless,

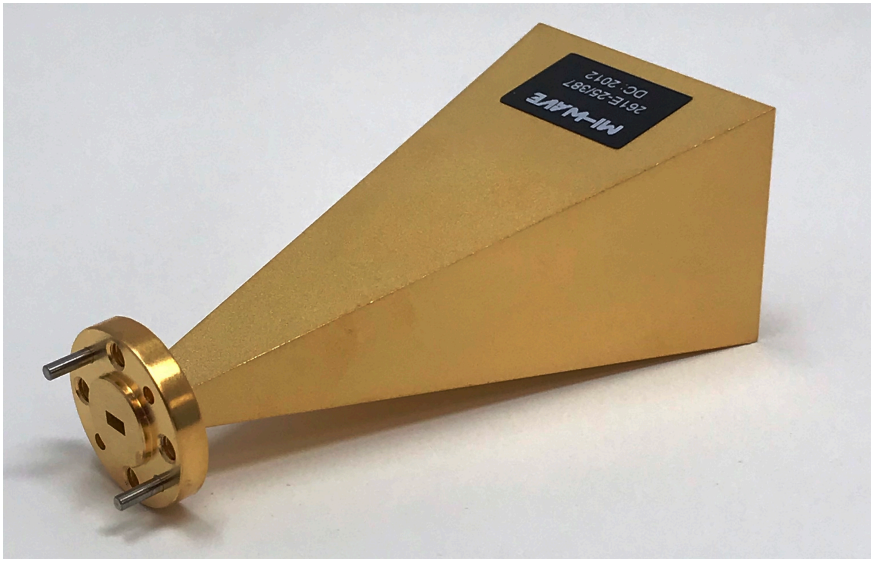


Figure 4.4: A picture of the Mi-Wave E-band antenna from [55] with a UG-387/U Flange type that has a gain of 25 dBi. It was used as the RF input into the downconverter.

Inc. [56], shown in Figure 4.5. It has a frequency range of 11.6 GHz to 13.9 GHz, which is within the range needed to provide the appropriate local oscillation for the downconverter. The step size for changing frequencies is 1 kHz. The frequency synthesizer is able to be controlled via a laptop and a USB connection, although a 5 line serial connection is also possible. The MLSP1113 also needed two 5 V and two 15 V power supplies with a current requirement of 300 mA and 1400 mA, respectively. The different configuration options for the frequency synthesizer were whether to include a 100 MHz reference signal, or a port where an external reference signal could be attached. The decision was made to include an internal reference signal, so that another component would not need to be added. Due to the inclusion of the internal reference signal, the current requirement for the frequency synthesizer would need an additional 125 mA for a total current of 1825 mA needed to power the device. The RT-65C 5 V/15 V power supply from Mean Well [57], shown in Figure 4.6, was chosen since it could provide both a 5 V power supply at a maximum current of 8000 mA, and a 15 V power supply at a maximum current of 2200 mA.

The last component in the system is the Agilent CSA Spectrum Analyzer N1996A, which

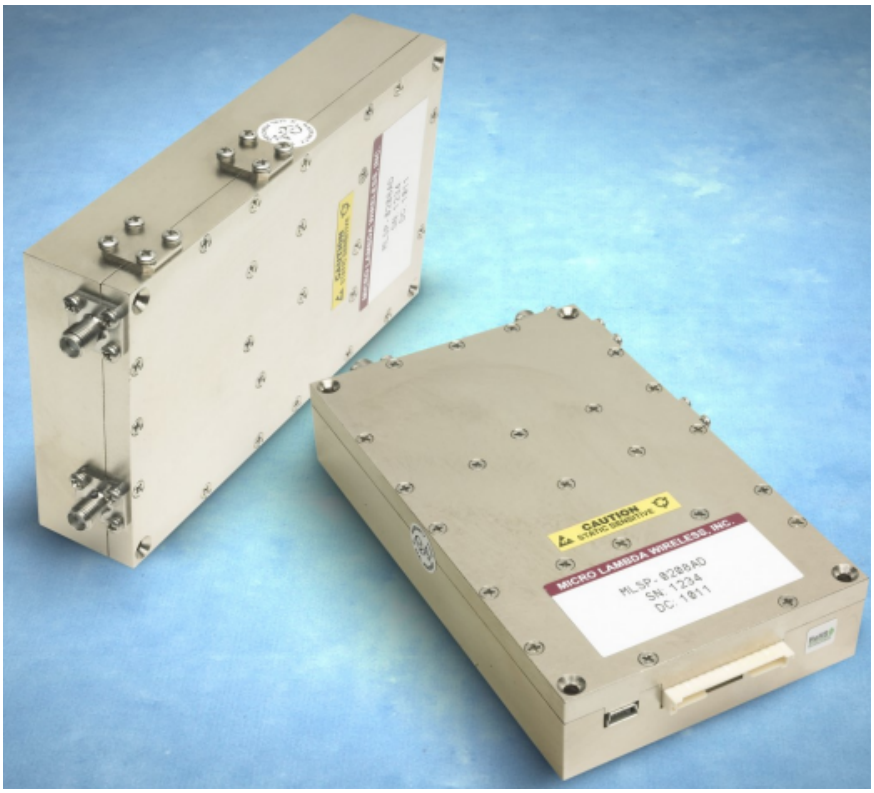


Figure 4.5: A picture of the Micro Lambda Wireless, Inc. MLSP1113 frequency synthesizer from [56]. It has an operating range of 11.5 GHz to 13 GHz.

would be used to visualize the signal power [59]. It is shown in Figure 4.7. It operates in the frequency range of 100 kHz to 3 GHz, which is within the 1 GHz to 2 GHz range of the output signal from the downconverter. A 3 dB attenuator, specifically the PE70A1009 from Pasternack, was also chosen to be put before the spectrum analyzer to mitigate the risk of any damage.

## 4.2 Measurement Platform Structure

The first step in combining the components into one cohesive measurement platform was to figure out the power configuration of the system; the final result is shown in Figure 4.8. Each of the three power supplies had an input for an AC 120 V line, an AC Neutral line, and

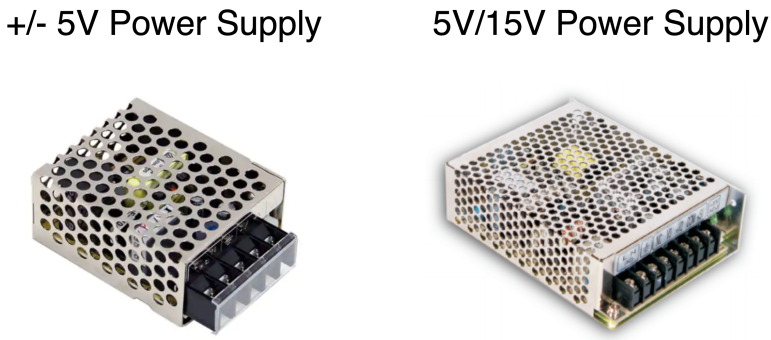


Figure 4.6: The two Mean Well power supplies are pictured above from [58] and [57] respectively. The RS-15-5 was the power supply used for the -5 V and +5 V to the downconverter. The RT-65C outputted the 5 V and 15 V necessary for powering the frequency synthesizer.


Figure 4.7: A picture of the Agilent CSA Spectrum Analyzer N1996A. It operates from 100 kHz to 3 GHz.

a field ground line. They then output the respective DC voltages; 5 V for the downconverter, -5 V for the downconverter, and 5 V and 15 V for the frequency synthesizer. The inputs to

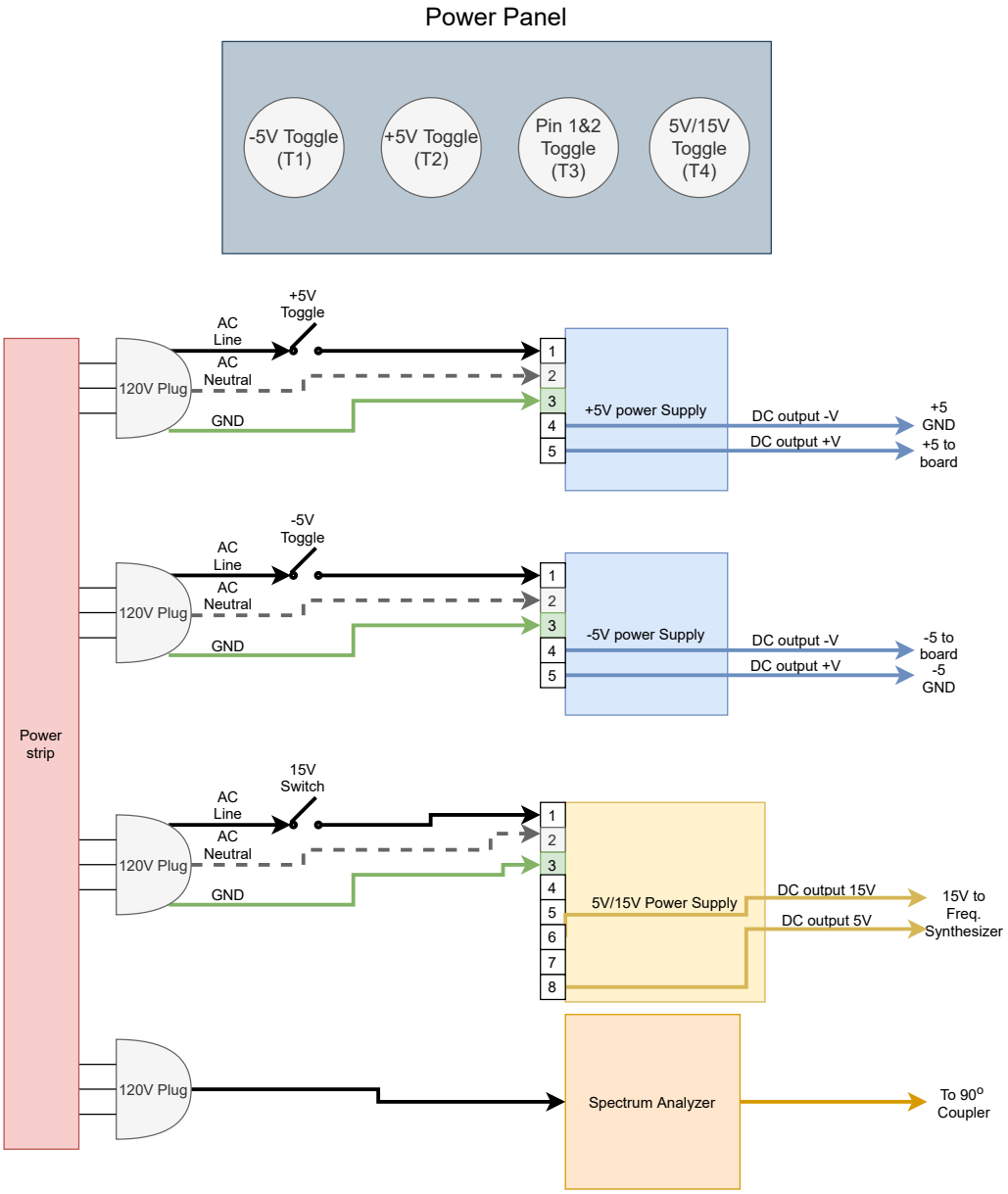


Figure 4.8: A detailed illustration of the power configuration for the measurement platform. The panel shows the toggles in the order they must be flipped to "ON" to safely power up the downconverter.

the power supplies were combined onto a power strip so that one external 120 V plug could be used to power all the components. Toggles, as shown in Figure 4.9, were added to be able to switch the AC line on and off for all the devices, due to the downconverter start up sequence requirement. This allowed the -5 V to the downconverter to be turned on first, followed by the +5 V, also to the downconverter. Another toggle was added for the pin 1 and pin 2 connection in order to eliminate the need to place a jumper on and off the pins for each power on and power off. The last toggle was for the frequency synthesizer, which needed to be turned on last during the power up sequence. The toggles were placed on a panel in the order that they would need to be flipped on; the reverse order could then be used to safely power down the downconverter.

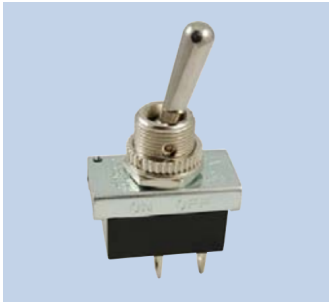

Figure 4.9: A picture, from [60], showing the NTE Electronics, Inc. 54-738 toggles used to control when devices were powered up without using separate external power supplies for all the components that needed a power supply.

After the power configuration of the measurement platform was determined, the next step was to configure the connectors for each device. The antenna was attached to the WR-12 waveguide on the back of the downconverter with dowels. The LO input on the downconverter was a 2.92 mm female connector and the frequency synthesizer output was a SMA female connector. In order to connect these two components, a 2.92 mm Male to SMA female adaptor was attached to the LO input connection, so that a SMA male to male cable could be used to join the frequency synthesizer to the LO input. All four downconverter outputs were SMA female connections, as were all the connectors on the 180° hybrid couplers and the 90° hybrid coupler. This meant that SMA male to male

cables could be used to join the downconverter outputs to the 180° hybrid couplers to the 90° hybrid coupler.

The 3 dB attenuator had a SMA female connection that could be connected to the 90° hybrid coupler via a SMA male to male cable. The other connector type on the attenuator was a SMA male, and the connector input to the spectrum analyzer was a N female type. A N male to SMA female adaptor was used to connect the attenuator to the spectrum analyzer. The impedance of the SMA cables, components, and the attenuator were all matched to 50 Ohms. The cables from the output of the downconverter were chosen to be able to handle at least 2 GHz. The cable connecting the frequency synthesizer to the LO input was chosen to be able to handle at least 14 GHz. After choosing all of the connectors, the system configuration was complete. A block diagram is shown in Figure 4.10. A step by step guide to connecting all the components of the measurement platform is given in Appendix B.

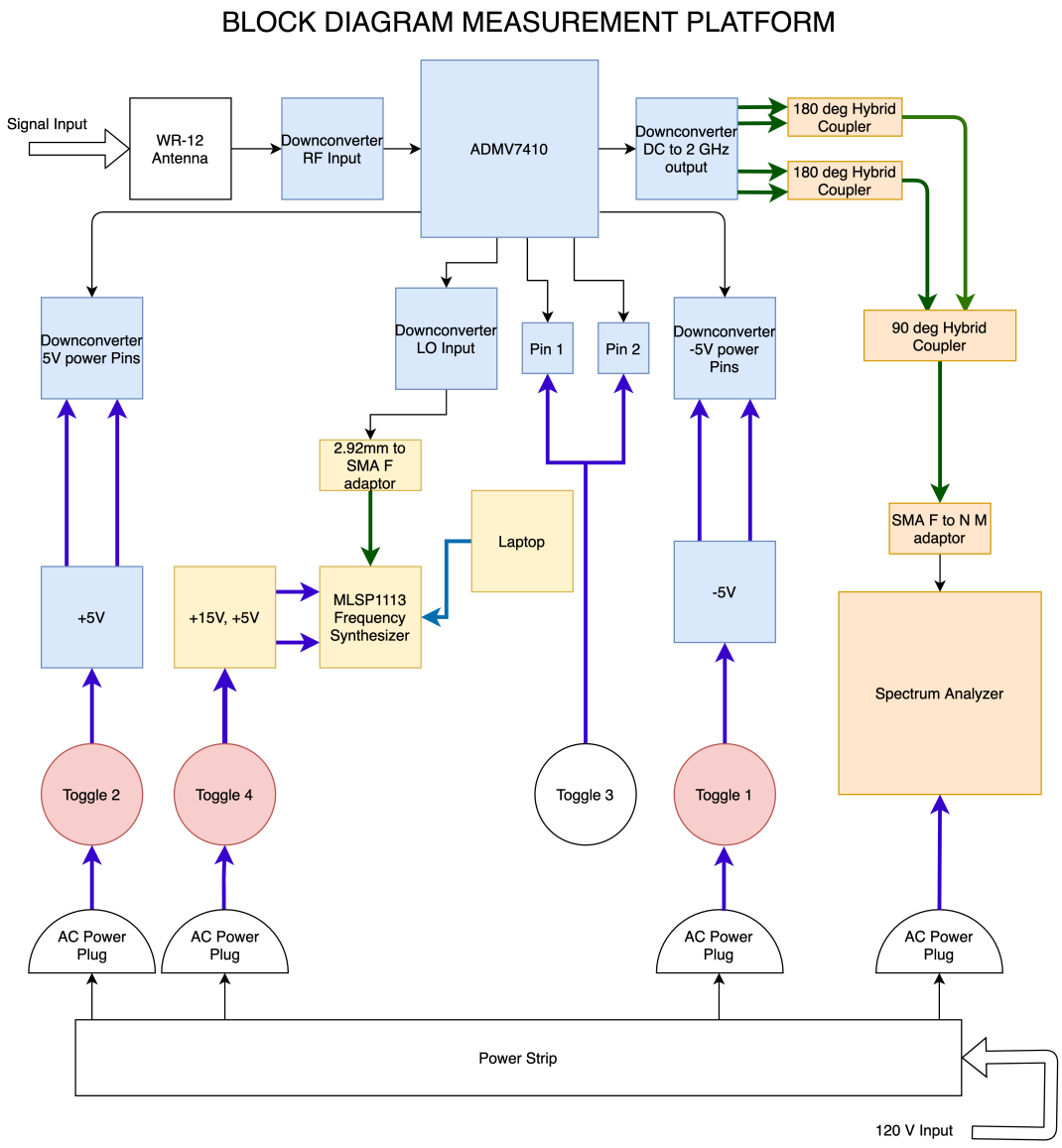


Figure 4.10: A complete block diagram of the measurement platform. The blue indicates all components that are on the downconverter or that directly connect to it. The orange indicates the path of the received signal to the spectrum analyzer. The yellow indicates components that directly connected to the frequency synthesizer. The red indicates components that related to the powering up of the downconverter. The white arrows are external inputs that had to be put into the system. The green arrows are SMA cable connections. The purple arrows are wire connections. The black arrows indicate that those two blocks were either soldered or connected directly. The blue arrow is a USB connection to control the frequency synthesizer from a laptop.

## 4.3 System Link Budget and Signal-to-Noise Radio Analysis

A link budget analysis is included to estimate the theoretical performance of the measurement platform. The signal-to-noise ratio is then calculated to show that the received signal would be able to be differentiated from noise. The calculations are completed assuming a bandwidth of 125 MHz, a frequency of 74.375 GHz, a distance of 12.65 m, and a transmit power of 0 dBm. The main components of the link budget analysis are given in Table 4.2. These values can then be used to calculate the link budget:

$$(P_{Rx})_{dBm} = (P_{Tx})_{dBm} + (G_{Tx})_{dBi} + (G_{Rx})_{dBi} + (G_C)_{dB} - (L_s)_{dB} - (L_a)_{dB} = -8.726\,dBm,$$

where $L_a$ includes all the insertion losses and other power losses. To check the signal-to-noise ratio (SNR), the thermal power noise can be calculated with the equation:

$$P_n = 10log_{10}(kBT/1mW) = -93.03\,dBm$$

where $k$ is Boltzman's constant, $T$ is the temperature in Kalvin (which is 293 K for room temperature), and $B$ is the bandwidth of the signal. The typical noise figure of the downconverter is found to be 5 dB from the data sheet. Overall, this means the SNR is:

$$SNR_{dB} = (P_{Rx})_{dB} - ((P_n)_{dB} + N_{dB}) = 82\,dBm,$$

where $N$ is the noise figure and was found in the downconverter data sheet. This indicates that the receiver should be able to distinguish the signal from the noise, since this is a large SNR value. These calculations are theoretical, and performance of the measurement platform will mostly likely vary from these values.

Table 4.2: The values used for the link budget analysis.

| | |
|---|---|
| Transmit Power ($P_{TX}$) | 0 dBm |
| Transmitter Antenna Gain ($G_{TX}$) | 43 dBi |
| Free Space Path Loss ($(L_s)_{dB}$) | 83.91 dB |
| Receiver Antenna Gain ($G_{RX}$) | 25 dB |
| Downconverter Small Signal Conversion Gain ($G_C$) | 13 dB |
| 180 deg coupler, insertion loss | 1.3 dB |
| SMA cables to 180 degree couplers, insertion loss | 0.283 dB |
| SMA cable to 90 degree coupler, insertion loss | 0.283 dB |
| SMA cable to attenuator | 1 dB |
| N to SMA Adaptor | 0.1 dB |
| Attenuator | 3 dB |

## 4.4 Outdoor Enclosures

The millimeter wave commercial radio links were built outside. Consequently, this measurement platform had to also be able to go outside with a minimal risk of damage. The Siklu radios were approximately 7 ft in height, and since it would be too difficult to use the measurement platform if all the components were up in the air, the system was split and two different enclosures were built. The major components in one of the enclosures contained the downconverter, couplers, and antenna, while the other contained the power supplies, frequency synthesizer and spectrum analyzer. The enclosure with the antenna was up 7 ft off the ground so that it would be able to receive signals from the Siklu radios. The enclosure with the spectrum analyzer was near the ground, where everything would be accessible. As a result, the power supply wires to the downconverter, the SMA cable from the spectrum analyzer to the 90° hybrid coupler, and the SMA cable from the frequency synthesizer to the LO input on the downconverter all needed to be around 7 ft long in order to reach the enclosure containing the downconverter.

The lower enclosure was a weatherproof box with a lid. Holes were made for the external

power supply wires and the frequency synthesizer SMA cable. The spectrum analyzer was placed face up so that it would be easily accessed when the lid was open. The upper enclosure was also plastic and had a removable lid. The inside of each enclosure is shown in Figure 4.11 and Figure 4.12.

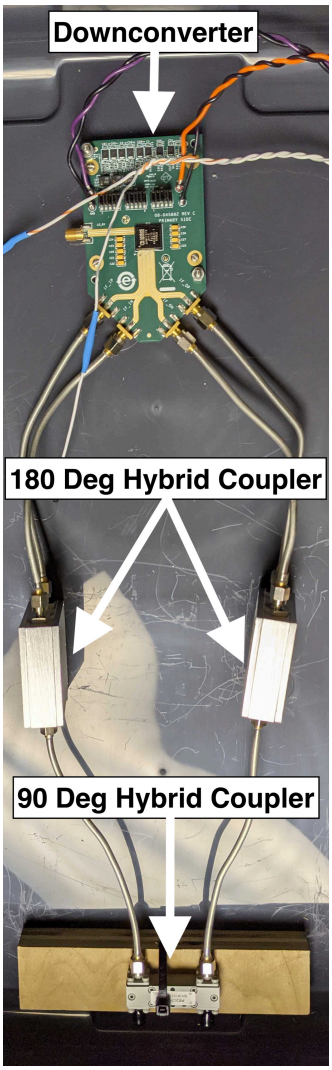


Figure 4.11: A picture of the enclosure with the downconverter. The antenna was opposite the downconverter chip. This enclosure was 7 ft from the ground so that the antenna could be aligned with a Siklu radio antenna.

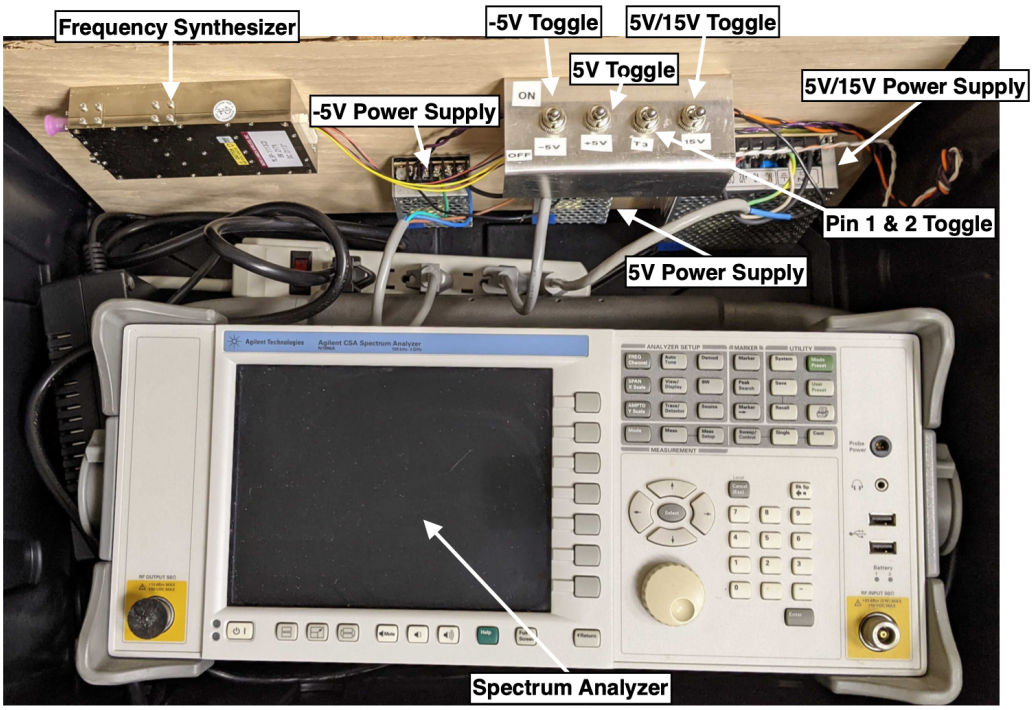


Figure 4.12: A picture of the inside of the enclosure that was close to the ground. This is where the downconverter could be powered on and where the signal could be seen on the spectrum analyzer.

## 4.5 Summary

This chapter went into detail about the measurement platform's overall configuration. The downconverter was the main component that the rest of the system was built around. The other major components chosen were the WR-12 antenna, couplers, and frequency synthesizer. The power supply setup was also explained, and resulted in just one external power supply being needed to power the whole system. A link budget analysis was also included to give a baseline expectation of performance. Lastly, details about the two outdoor enclosures that held all the measurement platform's components was given.

# Chapter 5

# Proof-of-Concept Measurement Results

This chapter details the process of making measurements to show that the receiver system could detect and visualize signals at the E-band frequency. For this specific experiment, measurements were taken at 71.937 GHz. An overall image of the measurement platform is shown in Figure 5.1. The setup, procedure, and results are provided in the following sections.

## 5.1 System Setup

Once the enclosures and equipment had arrived, there were a few more steps to complete before the receiver system was ready to be utilized to make measurements. Mainly, the last two SMA cable connections, one from the LO input of the downconverter to the frequency synthesizer, and the other from the 90° coupler output to the spectrum analyzer, had to be attached. The necessary software was installed onto a laptop in order to control the frequency synthesizer. This was done by using the software that was included with the hardware via CDROM disk.

The first test to see if the receiver system was set up correctly was to try to power it on. This was completed by following the power sequence: (i) flip the -5 V toggle to “ON”,

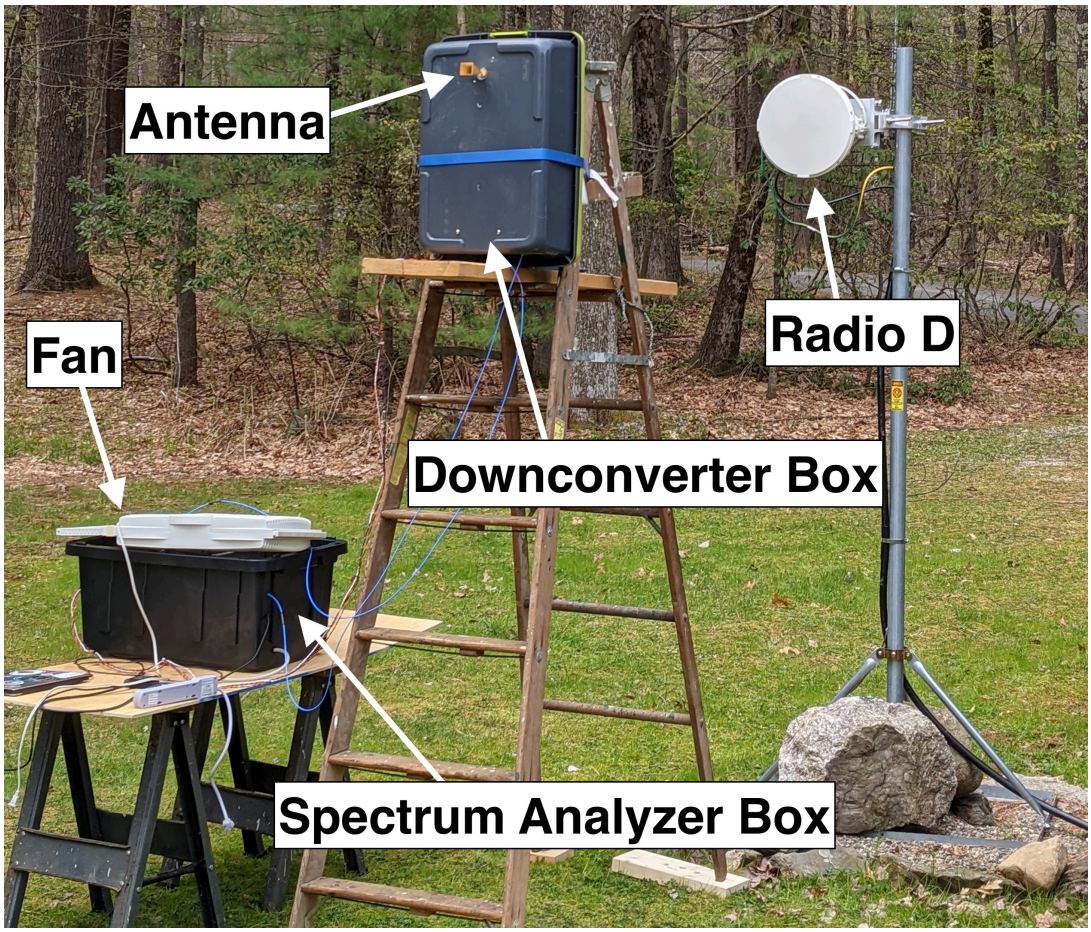


Figure 5.1: An image of the experiment setup when the receiver system was facing Radio C. The downconverter box was on top of a ladder and supported by a piece of plywood and held on with straps. A fan was added on top of the spectrum analyzer system to prevent the frequency synthesizer from overheating.

(ii) wait 30 seconds, (iii) flip the 5 V toggle to "ON", (iv) flip the T3 toggle to "ON", (v) and then flip the 15 V toggle to "ON". This sequence was to first input the -5 V to the downconverter, then input the 5 V to the downconverter, next connect pins 1 and 2 on the downconverter, and finally turn on the frequency synthesizer. This sequence had to be carefully followed in order to avoid damage to the downconverter. Once the system was powered, the frequency synthesizer had to be configured to the correct $f_{LO}$ value. It was decided to use the radio link from Radio C to Radio D as there was flat ground between this link, whereas the other radio link was on a sloped surface. The Radio C to Radio D link was set to a frequency of 71.9375 GHz or 71937.5 MHz, with a 125 MHz channel bandwidth. An $f_{IF}$ of 1500 MHz was chosen, as that was the center frequency of the hybrid couplers, and would therefore ensure that none of the signal could get attenuated. The $f_{LO}$ was then calculated, keeping in mind that the downconverter used a 6x LO multiplier:

$$f_{IF} = f_C - 6f_{LO} \rightarrow f_{LO} = \frac{f_C - f_{IF}}{6} = \frac{(71937.5 - 1500)\,MHz}{6} = 11739.6\ MHz$$

which meant that the frequency synthesizer would need to be set to a frequency of 11739.6 MHz. The frequency synthesizer computer interface is shown in Figure 5.2. Commands were sent by inputting the necessary commands in the "ASCII" inbox and then pressing "Send Command". If the command requested information, such as the max temperature the device had reached, the answer would appear in the interface under "ASCII Char's Received". The frequency was shown under the "Frequency:MHz" label. The command: `F11739.6` was sent to the frequency synthesizer in order to change its frequency to the necessary $f_{LO}$ value. The temperature could also be monitored with the command `R0020`; this was important during experimentation in order to ensure the device did not exceed its limit of 60°C or 140°F. The frequency synthesizer could also be used in a sweep mode where it would go through a specified range of frequencies. This function was not utilized because only signals around 71.937 GHz were being tested and therefore only one local oscillator frequency was needed.

The next step was configuring the spectrum analyzer so that it could visualize the correct frequency interval, and subsequently be able to show the power levels of any received signals. The $f_{IF}$ was set to 1.5 GHz so that the expected downconverted signal would be at that

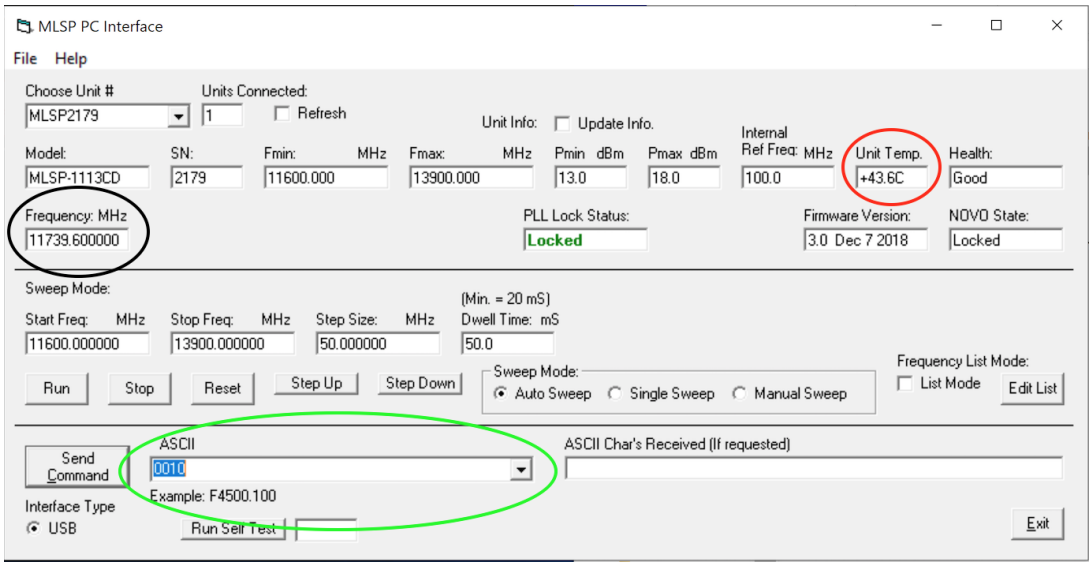


Figure 5.2: This is a screenshot of the frequency synthesizer computer interface. The frequency that the frequency synthesizer has been set to is circled in black. The black circle is where the internal temperature of the device can be monitored. The green circle indicates where to input commands, which are used to communicate with the device.

frequency; therefore, the center frequency of the spectrum analyzer was also set to that value. The resolution was set to 20 kHz. The channel bandwidth was 125 MHz, meaning that 71937.5 MHz, the center frequency, would be in the middle of that bandwidth. Once downconverted, the center frequency would be at the $f_{IF}$ of 1500 MHz and the channel bandwidth would stay at 125 MHz. Consequently, the equations used to calculate the start and stop frequency of the spectrum analyzer were:

$$f_{start} = f_{IF} - \frac{B_c}{2}$$

$$f_{stop} = f_{IF} + \frac{B_c}{2}$$

where $B_c$ is the channel frequency. The span of the spectrum analyzer was extended beyond this range to 220 MHz to ensure visualization of the full bandwidth of the signal. Once this was completed, the receiver system was ready to take measurements.

A final addition to the system was a large fan which would blow air into the spectrum

analyzer enclosure. The fan was added to prevent the frequency synthesizer from overheating and potentially being damaged. At one point the frequency synthesizer reached a temperature of around 147°F or 64°C, which was dangerous for the hardware, and it had to be turned off. This indicated that the frequency synthesizer was not in the most ideal placement. The synthesizer needed a heat sink to be able to cool properly. It was also found that the initial setup was attached to a piece of plywood, which is an insulator, so any heat that did build up was being retained. As a result the fan was added, and special attention was given to the internal temperature of the frequency synthesizer. The measurement platform was set up on a ladder, as shown in Figure 5.1.

## 5.2 Measurement Procedure

The procedure for making measurements with the receiver system was followed for each test case. There were a total of six configurations that were tested, and they are described in Table 5.1. During testing, the transmit power of the radio was varied from 0 dBm to -30 dBm in intervals of 10 dBm. The ladder that held the downconverter was rotated 180° to change between Radio D and Radio C being the transmit radio. The first configuration had the downconverter as close to the center of the antenna as possible in order to ensure that a signal could be detected. Subsequent tests were completed by moving the antenna to the left of the transmit antenna. Connection to the Siklu transmit radio was established via SSH to the corresponding server; an SSH command was executed again to connect to the radio itself. The transmit power was then modified using this command:

```
set rf tx-power POWER_LEVEL
```

Once the transmit power was set, a server and client connection using iPerf was completed as explained in Chapter 4, and data was transmitted over the line. Then a screenshot of the spectrum analyzer was taken.

Table 5.1: This table gives a number to the configurations that were attempted, and describes the position of the receiver system in relation to the transmit radio and the transmit radio's antenna.

| Configuration Number | Transmit Radio | Distance from Transmit Radio | Distance from bore sight of Transmit Radio |
|---|---|---|---|
| 1 | D | 5 ft | 0 ft |
| 2 | D | 5 ft | 1 ft |
| 3 | D | 5 ft | 2 ft |
| 4 | C | 85 ft | 0 ft |
| 5 | C | 85 ft | 1 ft |
| 6 | C | 85 ft | 0.75 ft |

## 5.3 Experimental Results

An image of the receiver system setup is illustrated for each of the six configurations that were tested. The results of the spectrum analyzer output are also shown for the corresponding transmit power. The center frequency for the spectrum analyzer was set to 1.5 GHz since the center frequency of the RF signal, at 71.937 GHz, was downconvertered to approximately 1.5 GHz.

Figure 5.3 shows the details of the first configuration, where the receiver system was put in front of Radio D at around 5 ft. This test was initially completed to see if a signal could be detected and visualized in the spectrum analyzer, and to also see how accurate the system was when the transmit power was modified. The result of the spectrum analyzer for this configuration when the transmit power was set to 0 dBm is shown in Figure 5.4. The center frequency was 1.5 GHz and the resolution bandwidth was 20 kHz. The bandwidth of the signal was approximately 125 MHz, and the whole signal was seen since the span was set to 220 MHz. The peak power spectral density was shown to be around -66.1 dBm. This indicates that the receiver system was able to receive and visualize a signal. The signal was quite noisy over the full bandwidth. This could have been caused by some of the components in the receiver system. Another explanation could be that the radio was constantly switching between transmitting and receiving faster than the spectrum analyzer sweep time, which was around 0.437 s. This would mean that the oscillation-like effect of

the signal could have been caused by the spectrum analyzer sensing when Radio D was receiving, which brought the power down, followed by the power being brought back up while Radio D was transmitting.

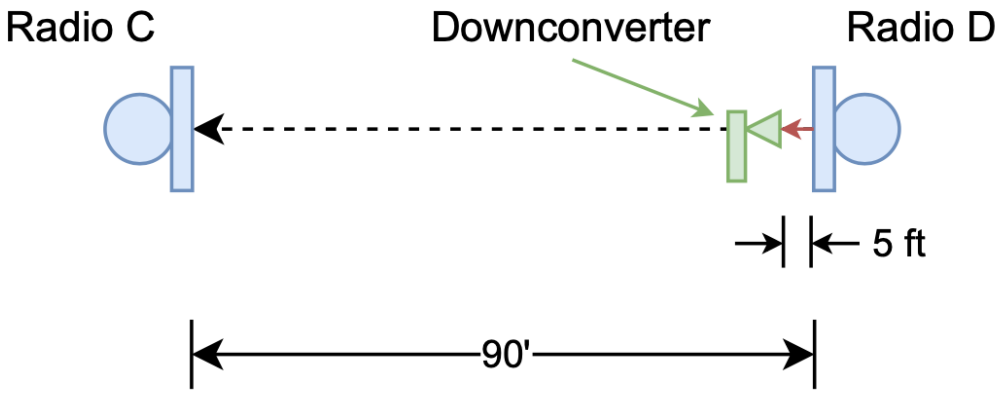


Figure 5.3: This diagram shows the first configuration for taking measurements. The downconverter was close to Radio D and was estimated to be at the center of the transmit radio's antenna.

The result of the spectrum analyzer for configuration one when the transmit power was set to -10 dBm is shown in Figure 5.5. The center frequency and resolution bandwidth remained unchanged at 1.5 GHz and 20 kHz, respectively. The bandwidth of the signal was approximately 125 MHz, and the whole signal was seen, since the span was set to 220 MHz. The peak power spectral density was shown to be around -73.1 dBm. This indicates that the receiver system was able to sense a decrease in transmit power of 10 dB. The result of the spectrum analyzer for configuration one when the transmit power was set to -20 dBm is shown in Figure 5.6. The center frequency and resolution bandwidth remained unchanged at 1.5 GHz and 20 kHz, respectively. The bandwidth of the signal was approximately 125 MHz, and the whole signal was seen, since the span was set to 220 MHz. The peak power spectral density was shown to be around -85 dBm. The signal continued to have the oscillation-like property, however, it was closer to the noise floor than when the transmit power was 0 dBm. This indicates that the signal, although still distinguishable

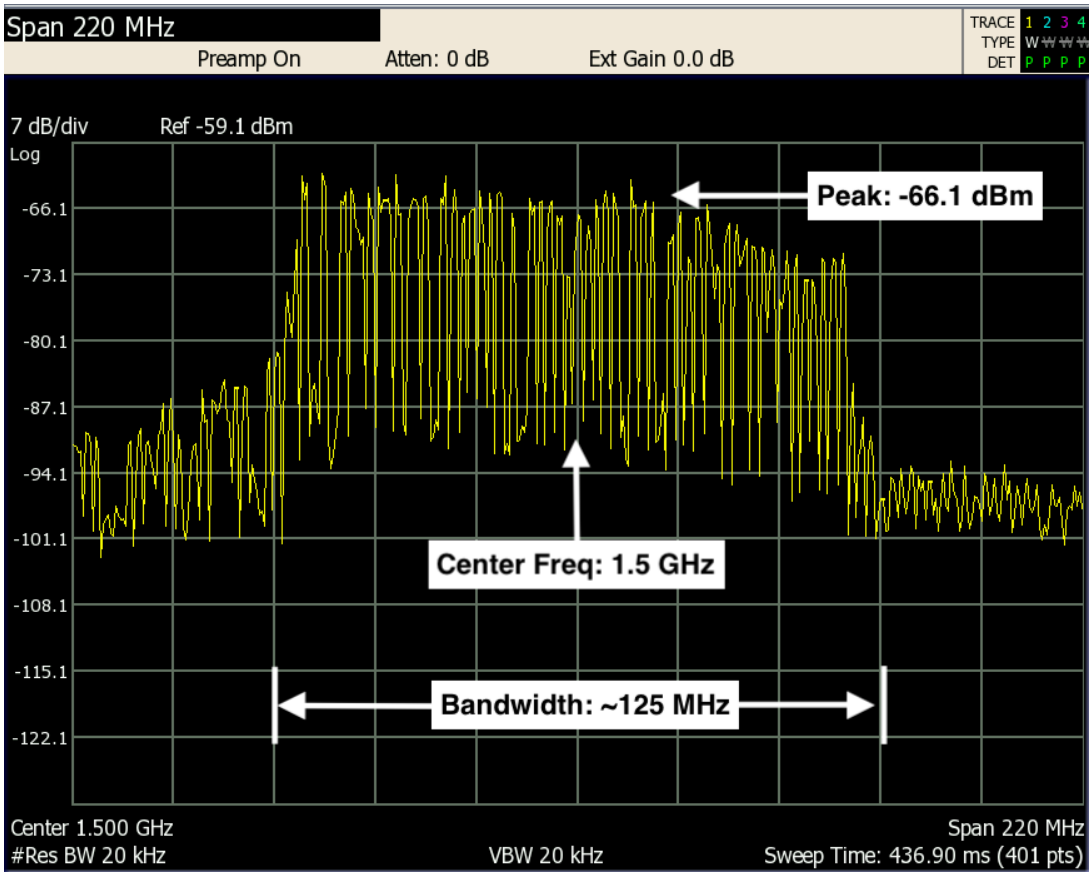


Figure 5.4: A screenshot of the spectrum analyzer output when the receiver system was in configuration one and the transmit power was set to 0 dBm. The peak power spectral density value is -66.1 dBm.

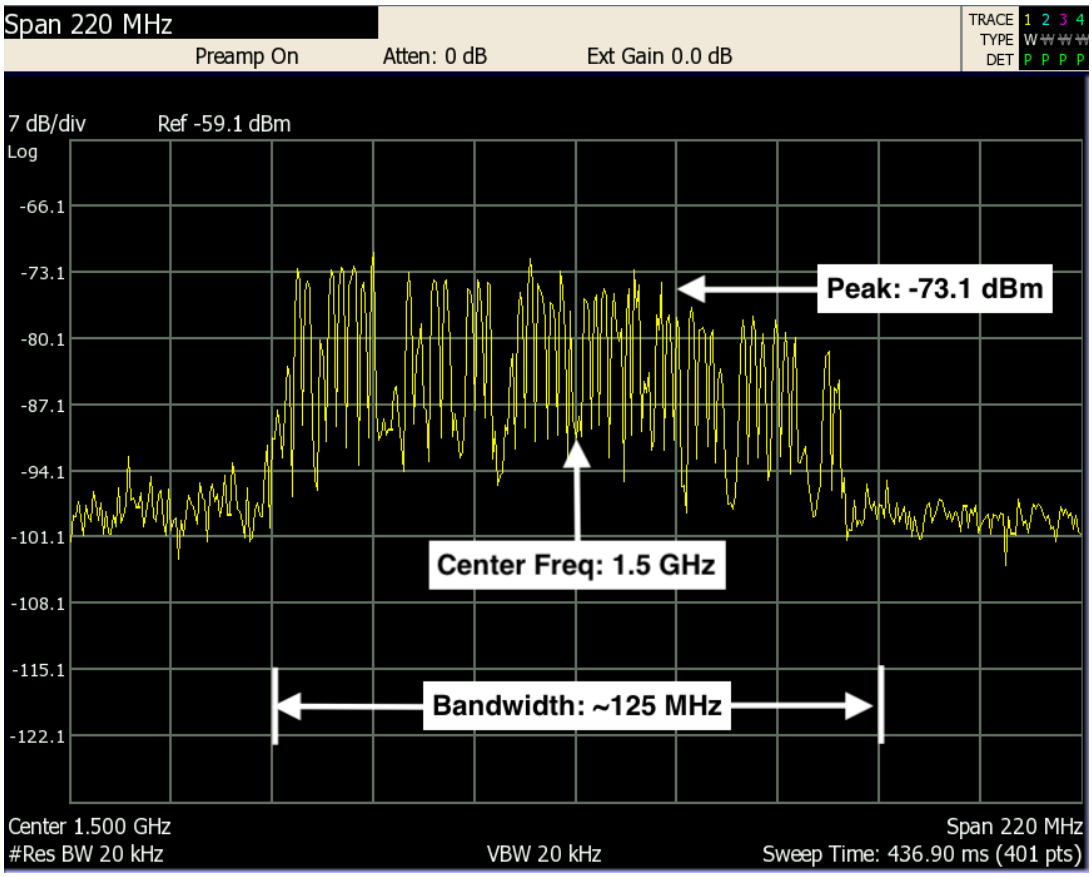


Figure 5.5: A screenshot of the spectrum analyzer output when the receiver system was in configuration one and the transmit power was set to -10 dBm. The peak power spectral density value is -73.1 dBm.

from noise, was becoming more difficult to detect. The result of the spectrum analyzer for configuration one when the transmit power was set to -30 dBm is shown in Figure 5.7. The center frequency and resolution bandwidth remained unchanged at 1.5 GHz and 20 kHz, respectively. The peak power spectral density was not determined since the result was only noise. This meant that the receiver was unable to detect a signal.

In order to check that these results were not outlandish, a link budget analysis was completed to compare them to theoretical values. However, the results of the measurements cannot directly be compared to the theoretical link budget analysis without accounting for some additional losses that occur due to how the signal is sent and how the spectrum analyzer operates. In order to create a foundation to calculate the theoretical loss, a transmit power of 0 dBm, which corresponds to 1 mW of power, needs to be assumed. Since the radio switches between receiving and transmitting for half the time, the power is cut in half. Theoretically, if the spectrum analyzer was directly connected to the transmitter without any additional system losses, 0 dBm would not be the peak power that could be reached. Rather, the spectrum analyzer shows power spectral density, which is power across a bandwidth. The reason for this is because the spectrum analyzer has a resolution bandwidth which acts as a filter across frequency and the power gets spread across this total bandwidth. For this particular experiment the resolution bandwidth was set to 20 kHz and the channel bandwidth was 125 MHz. To account for the losses the following formula can be used:

$$L = 10log_{10}\left[\frac{125\,MHz}{20\,kHz}\right] = 38\,dB$$

where $L$ is the expected loss for a received signal that is transmitted at 0 dBm just due to the spreading of the power across bandwidth and how the spectrum analyzer operates. An additional 3 dB of power loss is added since the radio only transmits half of the time. This means that the total loss that must be accounted for is 41 dB. Therefore, any peak power measurement shown at the output of the spectrum analyzer will actually be 41 dB lower than the theoretical received power from the link budget analysis. Considering this correction, Table 5.2 compares the theoretical link budget analysis values with the adjusted measurement results. The receiver system gains and losses for the link budget analysis are the same as those in Chapter 4 from Table 4.2. The free space path loss value had to be

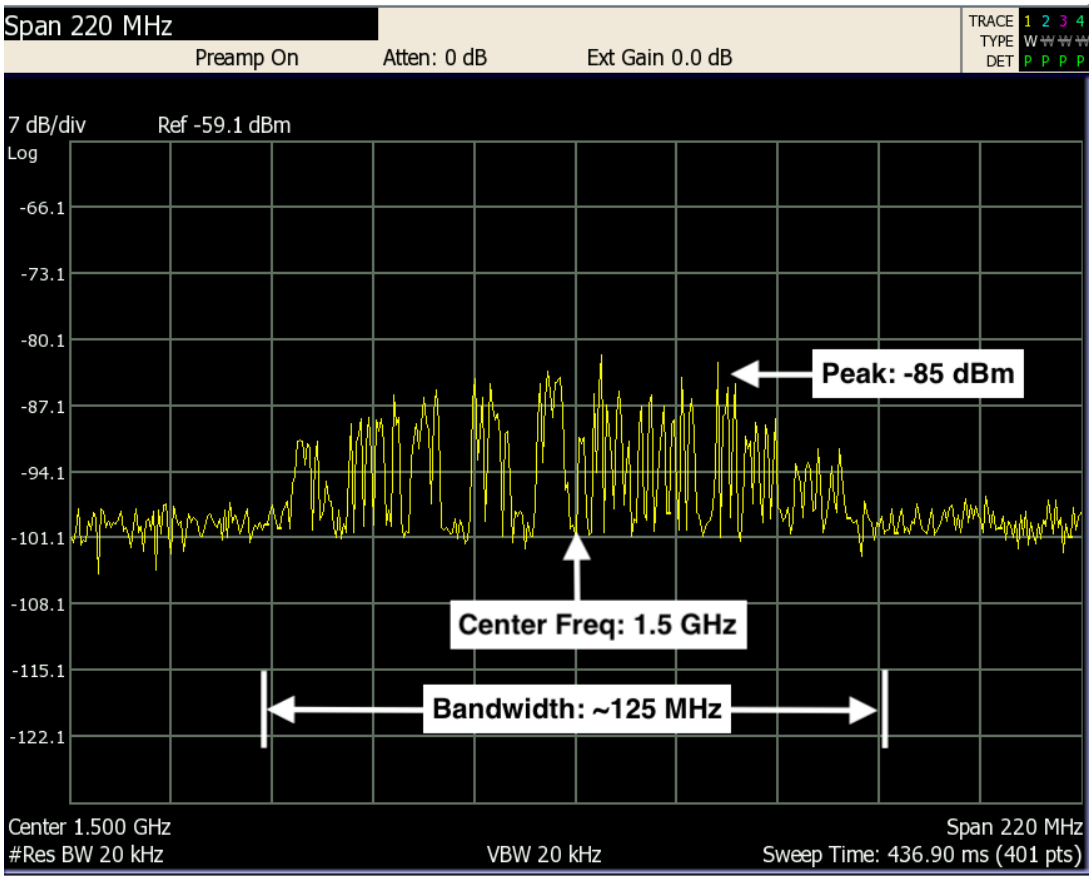


Figure 5.6: A screenshot of the spectrum analyzer output when the receiver system was in configuration one and the transmit power was set to -20 dBm. The peak power spectral density value is -85 dBm.

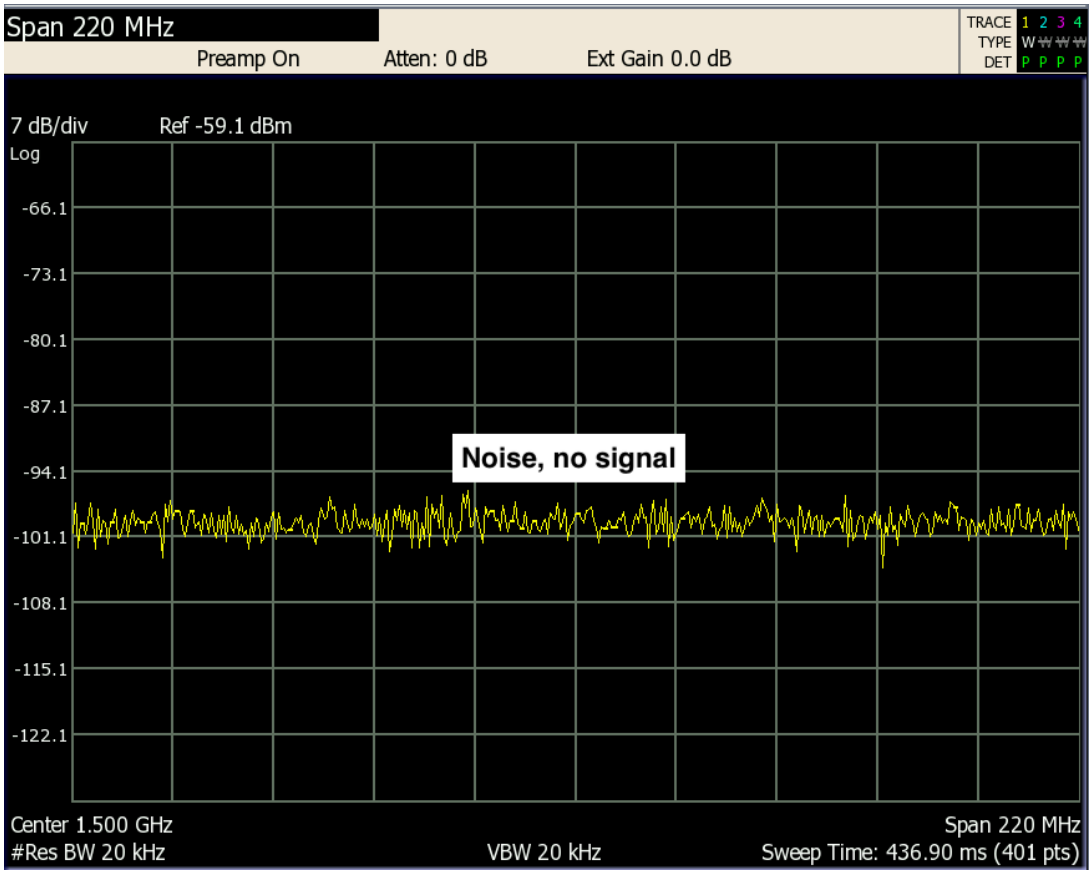


Figure 5.7: A screenshot of the spectrum analyzer output when the receiver system was in configuration one and the transmit power was set to -30 dBm. This output only shows noise, meaning that there was little to no received power.

recalculated to account for a frequency of 71.9375 GHz and a distance of 5 ft. The resulting free space path loss was 66.24 dB.

Table 5.2: A table comparing the theoretical received power to the adjusted for power loss due to how the spectrum analyzer displays signal power.

| TX Power (dBm) | Theoretical RX (dBm) | Corrected RX Measurement Results (dBm) |
|---|---|---|
| 0 | 8.944 | -28.1 |
| -10 | -1.056 | -35.1 |
| -20 | -11.056 | -47 |
| -30 | -21.056 | noise |

There is about a 32 dB difference in power when comparing the measured results to the theoretical values. This difference could be attributed to misalignment, since the receiver system was put at the estimated center of the Siklu antenna. This was approximated; a measurement device that would have ensured the receiver system was placed exactly at the center was not used.

The second configuration, shown in Figure 5.8, had the downconverter 1 ft to the left of the transmitter. This test was completed to see if any out-of-beam energy emissions from the transmitter could be detected with the receiver system. The result for a 0 dBm transmit power is shown in Figure 5.9. The center frequency and resolution bandwidth remained unchanged at 1.5 GHz and 20 kHz, respectively. The bandwidth of the signal was approximately 125 MHz, and the whole signal was seen, since the span was set to 220 MHz. The peak power spectral density was -94 dBm. This indicates that a shift of 1 ft from the center of Radio D's antenna caused the power of the received signal to decrease by approximately 28 dB.

The third configuration, shown in Figure 5.10, had the downconverter 2 ft to the left of the receiver. This test was completed to see if any out-of-beam emission could be detected when the receiver system was further misaligned with the transmit antenna. However, no signal was detected at the highest transmit power of 0 dBm; therefore, the spectrum analyzer result, shown in Figures 5.11, was just noise. This meant that the receiver was

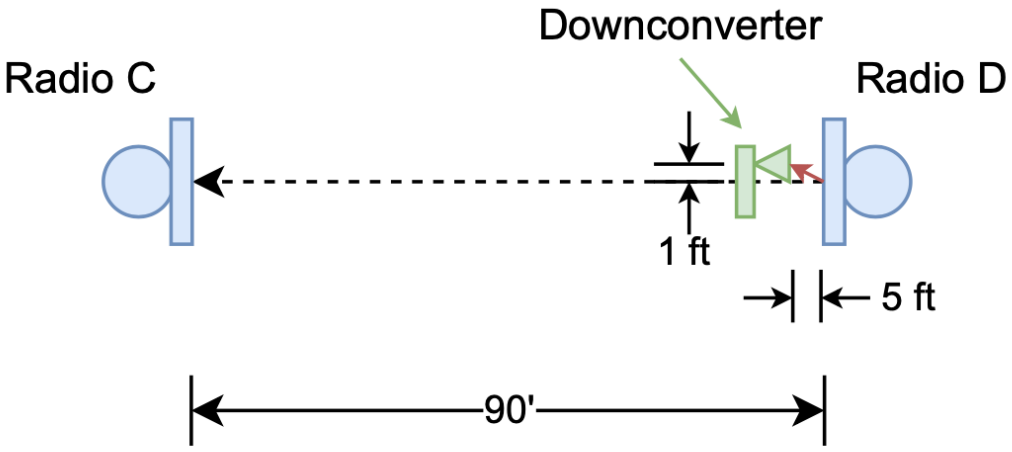


Figure 5.8: This diagram shows the second configuration for taking measurements. The downconverter was close to Radio D and was estimated to be 1 ft from the center of the transmit radio's antenna.

unable to detect a signal that could be distinguishable from noise and that a misalignment of 2 ft caused the transmitted signal to become undetectable.

The fourth configuration, shown in Figure 5.12, had the downconverter rotated 180°and moved to the estimated center of Radio C's antenna. This increased the distance from the transmit radio to the receiver system to 85 ft, so a lowered received signal power was expected given that more free space path loss occurs over a larger distance. The result for a transmit power of 0 dBm is shown in Figure 5.13. The center frequency and resolution bandwidth remained unchanged at 1.5 GHz and 20 kHz, respectively. The bandwidth of the signal was approximately 125 MHz, and the whole signal was seen, since the span was set to 220 MHz. The peak power spectral density was -83 dBm which was 17 dB lower than when the distance was only 5 ft in configuration one. This shows detecting a signal was becoming more difficult as the distance increased.

The result for configuration four when the transmit power was set to -10 dBm is shown in Figure 5.14. The center frequency and resolution bandwidth remained unchanged at 1.5 GHz and 20 kHz, respectively. The bandwidth of the signal was approximately 125 MHz,

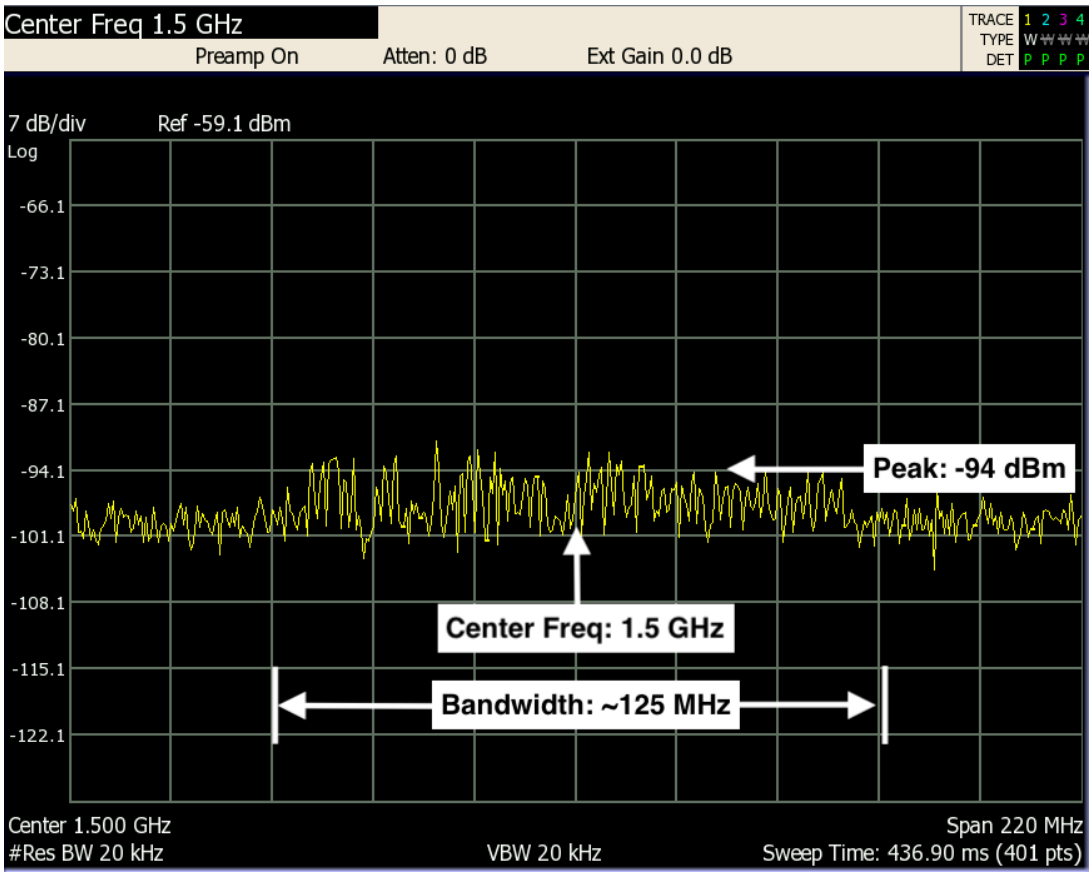


Figure 5.9: A screenshot of the spectrum analyzer output when the receiver system was in configuration two and the transmit power was set to 0 dBm. This output shows a peak power spectral density value of -94 dBm, which is lower than when the receiver system was in configuration one.

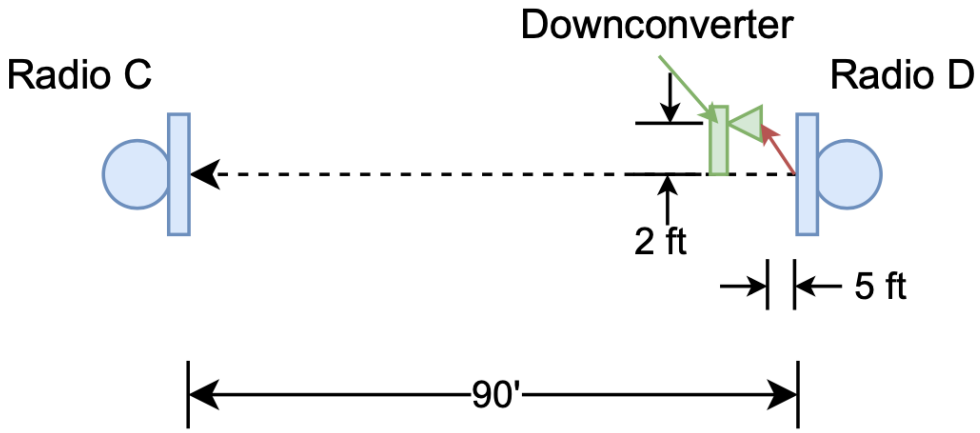


Figure 5.10: This diagram shows the third configuration for taking measurements. The downconverter was close to Radio D and was estimated to be 2 ft from the center of the transmit radio's antenna.

and the whole signal was seen, since the span was set to 220 MHz. The peak power spectral density value is shown to be -95 dBm. This indicated that the receiver was able to detect the signal at a lower transmit power level and greater distance. The detectable signal power was lower which is to be expected since the transmit power was decreased. For the next measurement, the transmit power was further decreased to -20 dBm, however, no signal was able to be detected as there was only noise.

The fifth configuration was when Radio C was the transmitter, and the receiver was 1 ft to the right of the center of Radio C's antenna. A signal could not be detected at 0 dBm with this configuration. The spectrum analyzer only showed noise. This configuration was modified, as shown in Figure 5.15, with the receiver antenna placed about 0.75 ft to the right of the transmit antenna's center. The spectrum analyzer result, when the transmit power was set to 0 dBm, is shown in Figure 5.16. The center frequency and resolution bandwidth remained unchanged at 1.5 GHz and 20 kHz, respectively. The bandwidth of the signal was approximately 125 MHz, and the whole signal was seen, since the span was set to 220 MHz. The peak power spectral density value is shown to be -90 dBm. This showed that the receiver was able to detect a signal at a greater distance even when the

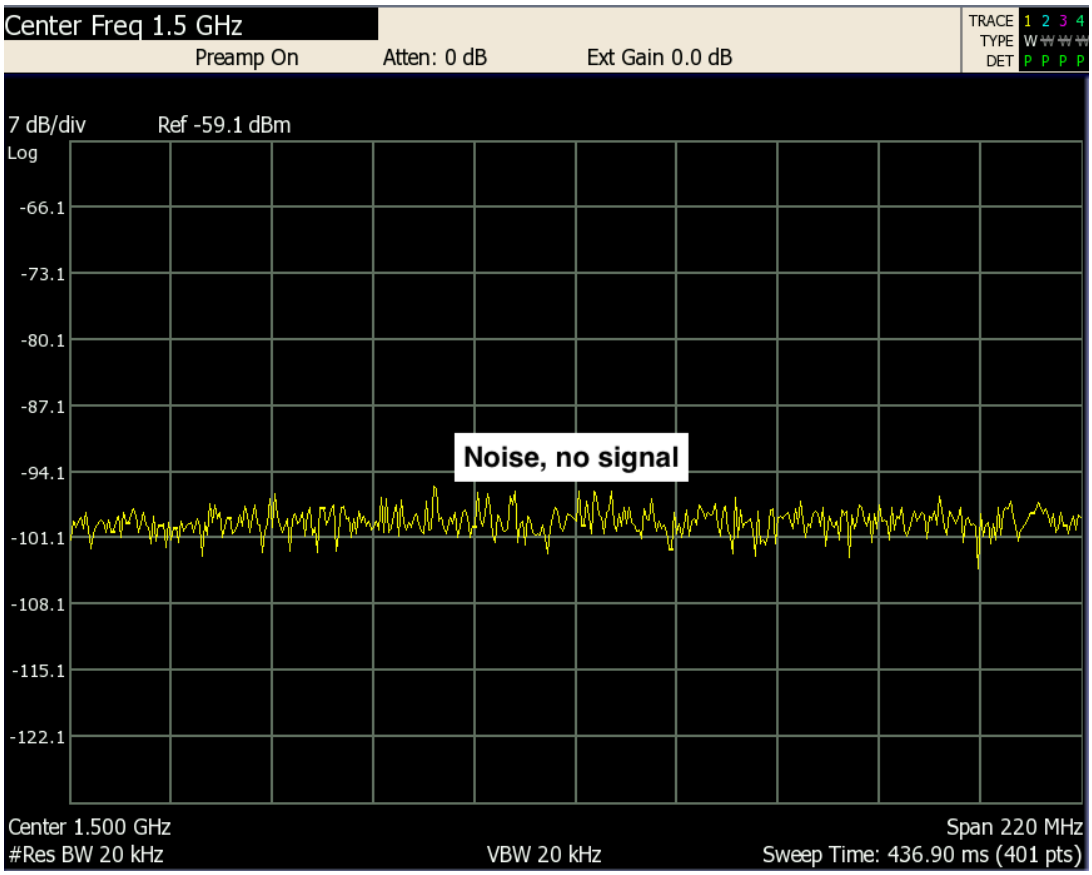


Figure 5.11: A screenshot of the spectrum analyzer output when the receiver system was in configuration three and the transmit power was set to 0 dBm. This output shows only noise. There is a slight power increase around the center frequency, but not enough to determine whether it is noise or a very weak received signal.

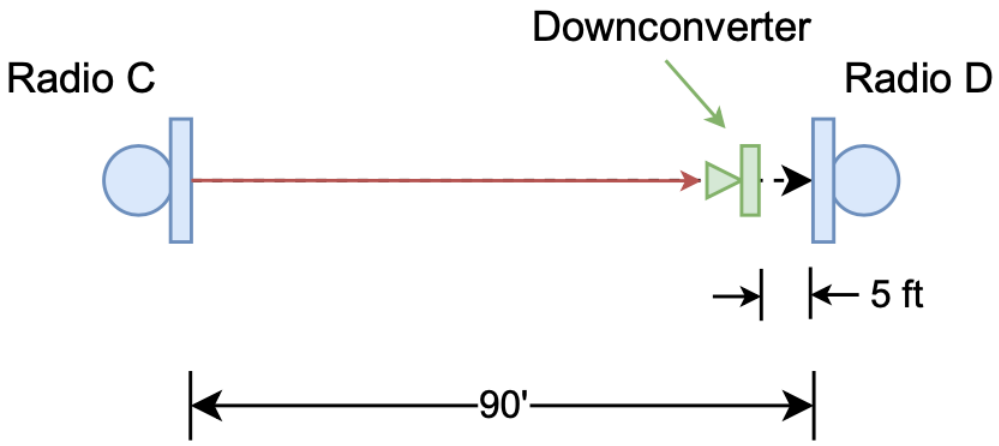


Figure 5.12: This diagram shows the fourth configuration for taking measurements. The downconverter faced Radio C and was estimated to be in line with Radio C's antenna.

antennas were misaligned. The spectrum analyzer result when the transmit power was set to -10 dBm is shown in Figure 5.17. The center frequency and resolution bandwidth remained unchanged at 1.5 GHz and 20 kHz, respectively. The signal was undetectable since it could not be distinguished from noise. This indicated that the receiver was able to detect out-of-beam emissions only for signals of relatively high transmit power.

The results are summarized in Table 5.3. It shows that the receiver system was able to receive and visualize a signal as shown by the first configuration test. It also confirms that the correct signal was being received, since when the transmit power was lowered by intervals of 10 dB, the received power also decreased in intervals of 10. The theoretical results from this configuration test were about 32 dBm more than the actual measured results. This could be attributed to misalignment, since the Siklu radios have such a narrow beamwidth, with a half power angle of 0.9°, and the receiver system antenna had a very small cross section, so perfect alignment without proper tools would have been almost impossible. However, other losses from either the transmit radio or the receiver system could also be explanations for the power difference. This can include things such as connectors and cables. The second configuration showed that when the receiver antenna was moved 1 ft to the left of the transmit antenna, some energy emission could still be detected, although it was low.

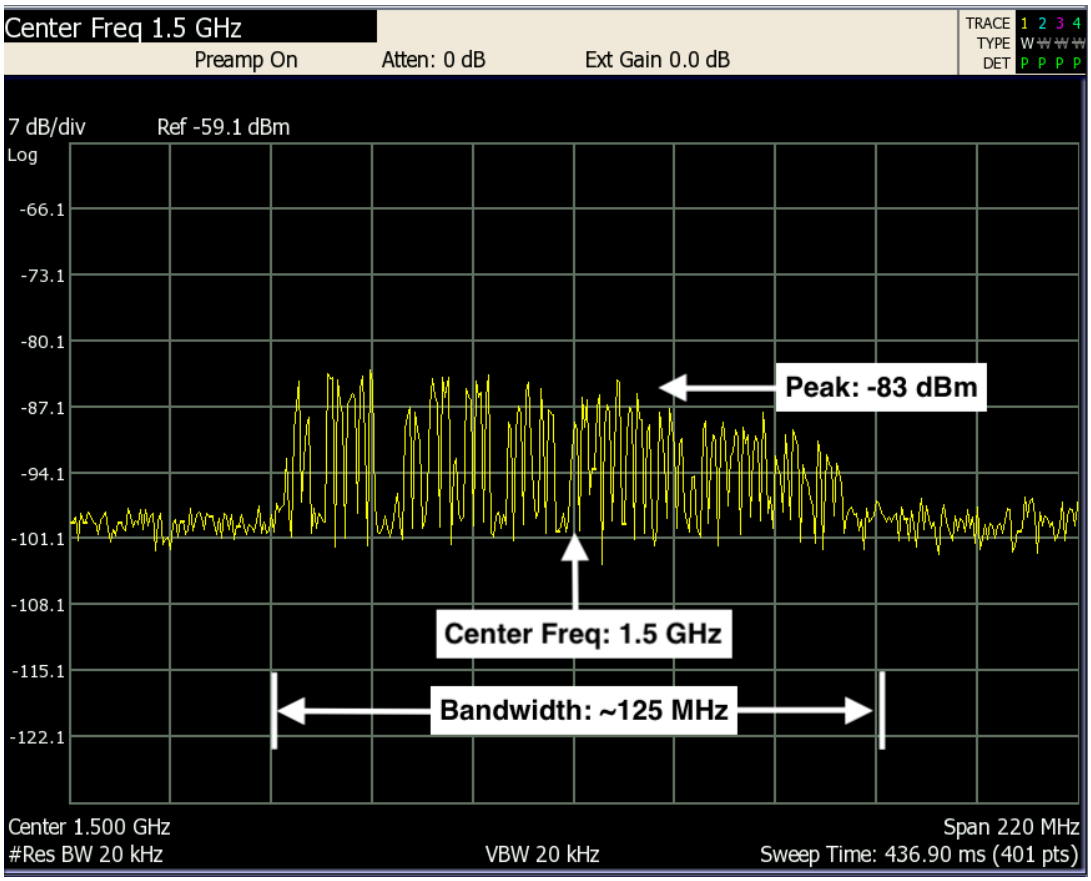


Figure 5.13: A screenshot of the spectrum analyzer output when the receiver system was in configuration four and the transmit power was set to 0 dBm. The peak power spectral density value is -83 dBm.

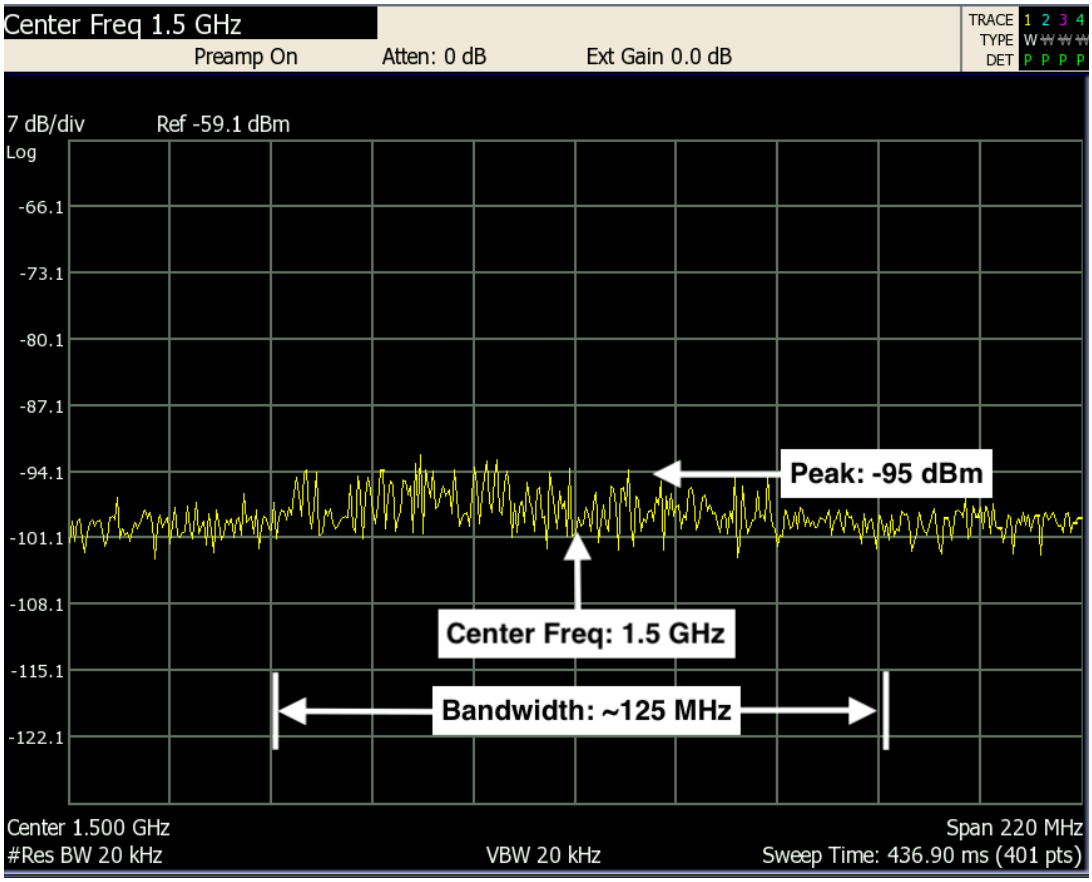


Figure 5.14: A screenshot of the spectrum analyzer output when the receiver system was in configuration four and the transmit power was set to -10 dBm. The peak power spectral density value is -95 dBm.

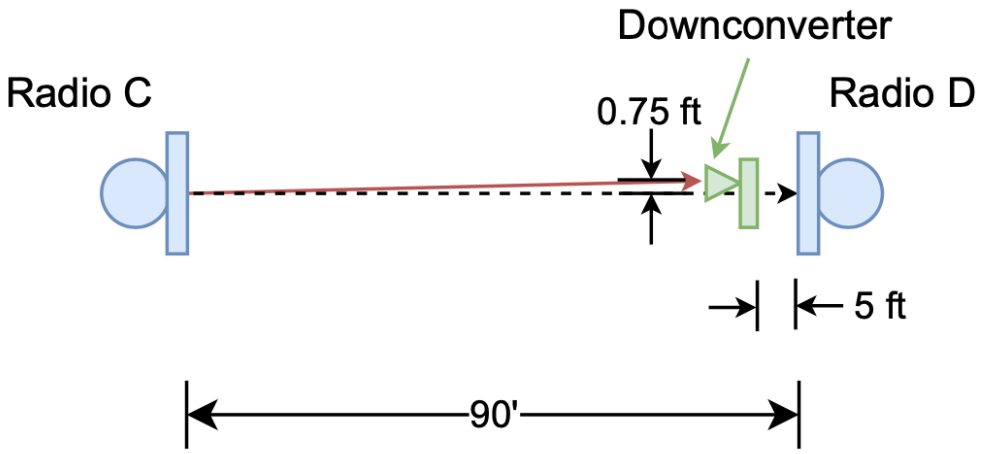


Figure 5.15: This diagram shows the sixth configuration for taking measurements. The downconverter faced Radio C and was estimated to be 0.75 ft to the right of the center of Radio C's antenna.

When the receiver antenna was further misaligned to be 2 ft from the center, there was no signal detection that could conclusively be distinguished from noise, even at a distance of 5 ft from the transmit antenna. When the receiver antenna was aligned with Radio C, the received signal power was 20 dB lower, which was expected due to an increased distance from the transmit radio to the receiver antenna. A misalignment of 1 ft from Radio C was too great, and no signal could be detected. As a result the receiver was moved to be just 0.75 ft to the right of Radio C. This change resulted in a signal being observed at about -90 dBm; however once the transmit power was lowered to -10 dBm, the signal was lost again.

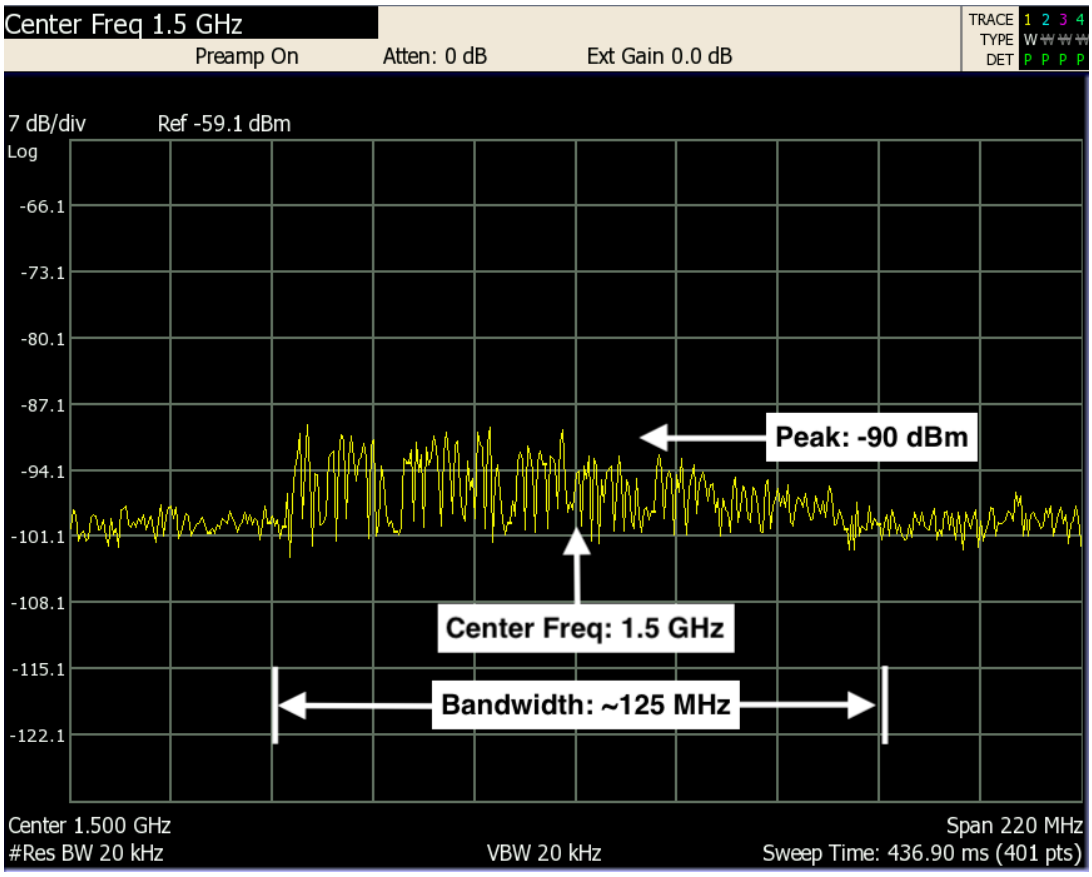


Figure 5.16: A screenshot of the spectrum analyzer output when the receiver system was in configuration six and the transmit power was set to 0 dBm. The peak power spectral density value is -90 dBm, which shows that the receiver system was able to detect a signal when its antenna was positioned 0.75 ft to the right of the center of Radio C's antenna.

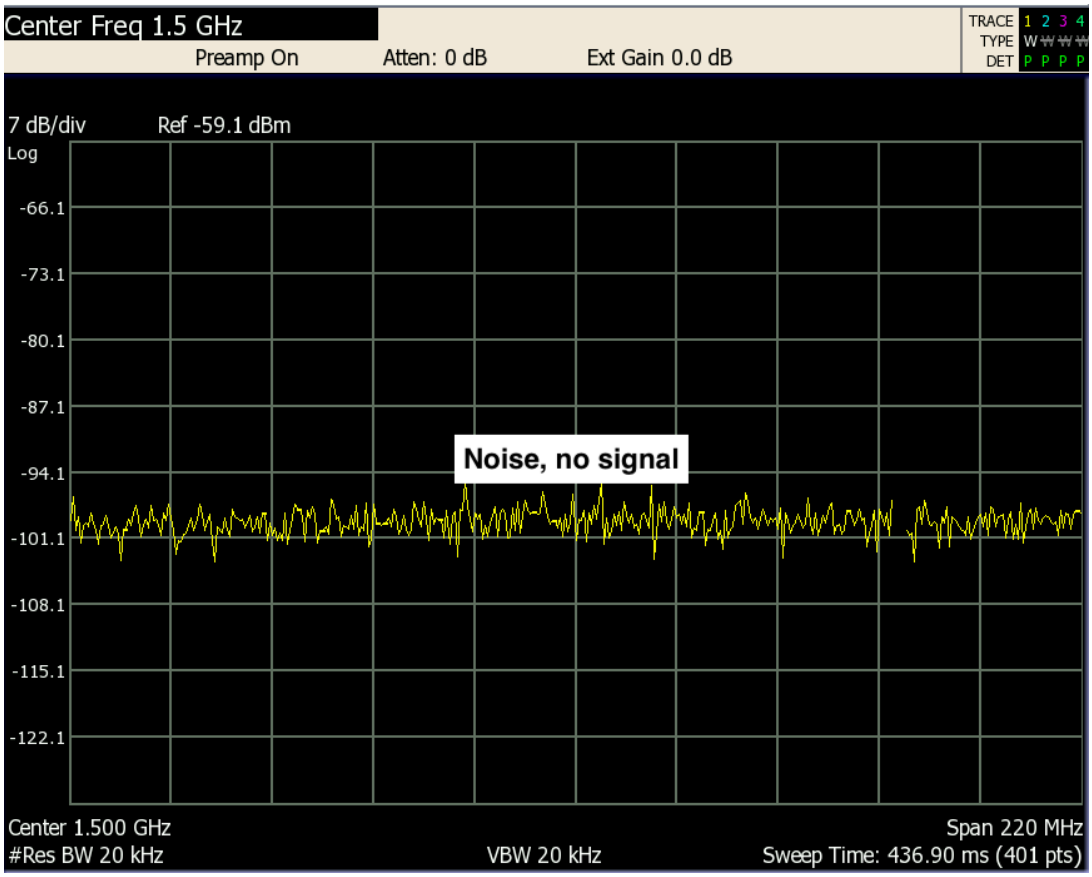


Figure 5.17: A screenshot of the spectrum analyzer output when the receiver system was in configuration six and the transmit power was set to -10 dBm. This output shows just noise, meaning that there was either a very weak or no received signal when the receiver antenna was 0.75 ft away from the center of Radio C's antenna.

Table 5.3: The configuration numbers, transmit powers, and measured peak power spectral density values are listed.

| Configuration Number | TX Power (dBm) | Peak RX Power (dBm) |
|---|---|---|
| 1 | 0 | -66.1 |
| | -10 | -73.1 |
| | -20 | -85 |
| | -30 | noise |
| 2 | 0 | -94 |
| | -10 | noise |
| 3 | 0 | noise |
| 4 | 0 | -83 |
| | -10 | -95 |
| | -20 | noise |
| 5 | 0 | noise |
| 6 | 0 | -90 |
| | -10 | noise |

## 5.4 Summary

In this chapter, the measurement setup, procedure and results were summarized. The setup mainly included configuring the frequency synthesizer, as well as discovering the need to dissipate the heat it generated, which resulted in the addition of a fan. The procedure that was used to make measurements included setting up the receiver in a particular place and then changing the transmit power, from 0 dBm to -30 dBm in intervals of ten, until no signal could be detected. In addition, iPerf was used to transmit data so that the maximum

channel bandwidth could be used and the transmitted data would be consistent. Overall, the results showed that the receiver system was able to visualize the signal, and out-of-beam energy emissions could be detected.

# Chapter 6

# Conclusion

This thesis focused on detailing a framework for an outdoor testbed that can be changed and adapted for future research on millimeter wave communication systems. The commercial radio configuration allowed for remote access so that work could be completed while not physically at the location of the testbed. A receiver system was built to detect out-of-beam energy emissions of the commercial millimeter wave testbed and initial measurement results were provided to show that it was functional. Overall, it was found that millimeter wave signals at 71.937 GHz could be detected even when the transmitter and receiver antennas were not aligned.

## 6.1 Research Outcomes

The general outcome of this thesis was an experimental framework for evaluating millimeter wave signal transmissions. Initial out-of-beam energy emission measurement results were given as a proof-of-concept to show that the testbed was functional. The following lists the three main outcomes from this thesis:

- A framework that can be used to build a remotely accessible outdoor millimeter wave testbed was provided. The rationale for all the decisions and the network configuration was also detailed so that any or all parts of the testbed can be replicated.
- A custom-built measurement platform was extensively detailed to enable the recre-

ation of the device. The rationale for all the components was provided so that if modifications to the systems are needed during replication, the guide could still be utilized to determine the important requirements and constraints that the receiver system needed to be built around.

- Initial proof-of-concept measurements of the measurement platform at 71.937 GHz showed that a signal could be detected when not completely aligned with a transmit antenna.

## 6.2 Future Work

There are many improvements that could be made to the testbed in order to expand the types of applications it can be used for. Also, more experimental measurements could be completed to further outline the out-of-beam energy emissions of millimeter wave signals in the E-band frequency range. The following lists possible areas where future work could be completed:

- Attempt to calibrate both the outdoor system and the receiver system to account for all power losses. A power loss of 20 dBm was shown between the Siklu radios and a power loss of 43 dBm was shown for the receiver system. While the main cause of this power loss was due to misalignment of the antennas, future work could determine if the cause was indeed misalignment, or rather issues within the Siklu radios or receiver system.

- Modify the enclosures in order to make them weatherproof enough to allow measurements to be taken in various weather conditions, without the concern that components could be damaged. Along with modifications to the enclosures, the measurement platform could also be modified to make it easier to move the downconverter and to more accurately measure the position of the receiver antenna in relation to the transmit antenna.

- Make more out-of-beam energy emission measurements at various frequencies ranging the full E-band of 71 GHz to 76 GHz. Additionally, more precise variations of distances

and angles from the transmit antenna would contribute to a comprehensive overview of the detectability of E-band signals.

# Bibliography

[1] Pew Research Center, "Internet/broadband fact sheet," https://www.pewresearch.org/internet/fact-sheet/internet-broadband/, 2021.

[2] ——, "Mobile technology and home broadband 2019," https://www.pewresearch.org/internet/2019/06/13/mobile-technology-and-home-broadband-2019/, 2019.

[3] ——, "53% of americans say the internet has been essential during the covid-19 outbreak," https://www.pewresearch.org/internet/2020/04/30/53-of-americans-say-the-internet-has-been-essential-during-the-covid-19-outbreak/, 2019.

[4] National Center for Education Statistics, "Distance learning," https://nces.ed.gov/fastfacts/display.asp?id=80.

[5] N. R. Council, *Networking Health: Prescriptions for the Internet*. Washington, D.C.: National Academies Press, 2000.

[6] Verizon, "What is millimeter wave technology?" https://www.verizon.com/about/our-company/5g/what-millimeter-wave-technology, online: accessed 05-1-2021.

[7] AT&T, "AT&T Rolls Out Super-Fast 5G+ Across the U.S." https://about.att.com/newsroom/2021/5g_plus.html, online: accessed 05-1-2021.

[8] T. S. Rappaport, S. Sun, R. Mayzus, H. Zhao, Y. Azar, K. Wang, G. N. Wong, J. K. Schuz, M. Samimi, and F. Gutierrez, "Millimeter wave mobile communications for 5g cellular: It will work!" *IEEE Access*, pp. 335–349, 2013.

[9] X. Wang, L. Kong, F. Kong, F. Qiu, M. Xia, S. Arnon, and G. Chen, "Millimeter wave communication: A comprehensive survey," *IEEE Communications surveys and tutorials*, vol. 20, no. 3, pp. 1616–1653, 2018.

[10] F. Register, "Permitting radar services in the 76-81 ghz band," https://www.federalregister.gov/documents/2017/09/20/2017-18463/permitting-radar-services-in-the-76-81-ghz-band, 2017.

[11] T. S. Rappaport, G. R. MacCartney, M. K. Samimi, and S. Sun, "Wideband millimeter-wave propagation measurements and channel models for future wireless communication system design," *IEEE Transactions on Communications*, vol. 63, no. 9, pp. 3029–3056, 2015.

[12] A. Quadri, H. Zeng, and Y. T. Hou, "A real-time mmwave communication testbed with phase noise cancellation," in *IEEE INFOCOM 2019 - IEEE Conference on Computer Communications Workshops (INFOCOM WKSHPS)*, 2019, pp. 455–460.

[13] G. K. Tran, M. Nakamura, H. Nishiuchi, K. Sakaguchi, R. Santos, and K. Koslowski, "Outdoor experiment of mmwave meshed backhaul for realtime edge content delivery," in *2019 IEEE Wireless Communications and Networking Conference Workshop (WCNCW)*, 2019, pp. 1–6.

[14] D. Steinmetzer, J. Chen, J. Classen, E. Knightly, and M. Hollick, "Eavesdropping with periscopes: Experimental security analysis of highly directional millimeter waves," in *2015 IEEE Conference on Communications and Network Security (CNS)*, 2015, pp. 335–343.

[15] Y. Zhu, Y. Ju, B. Wang, J. Cryan, B. Y. Zhao, and H. Zheng, "Wireless side-lobe eavesdropping attacks," 2018.

[16] T. Rappaport, *Millimeter wave wireless communications*, 1st ed. Upper Saddle River, N.J: Prentice Hall, 2014 - 2015.

[17] W. Stallings, *Data and Computer Communications*, 10th ed. Pearson, 2013.

[18] J. G. Proakis and M. Salehi, *Classical mechanics: the theoretical minimum*, 5th ed. New York, NY: McGraw-Hill, 2008.

[19] I. T. Union, "Attenuation by atmospheric gases," International Telecommunications Union, Tech. Rep. P.676-11, 2016.

[20] MathWorks, "Introduction to modeling the propagation of radar signals," https://www.mathworks.com/help/radar/ug/modeling-the-propagation-of-rf-signals.html.

[21] M. Marcus and B. Pattan, "Millimeter wave propagation: spectrum management implications," *IEEE Microwave Magazine*, vol. 6, no. 2, pp. 54–62, 2005.

[22] I. Shayea, T. Abd. Rahman, M. Hadri Azmi, and A. Arsad, "Rain attenuation of millimetre wave above 10 ghz for terrestrial links in tropical regions: A review study on rain attenuation of millimetre wave," *Transactions on emerging telecommunications technologies*, vol. 29, 2018.

[23] T. S. Rappaport, Y. Xing, G. R. MacCartney, A. F. Molisch, E. Mellios, and J. Zhang, "Overview of millimeter wave communications for fifth-generation (5g) wireless networks—with a focus on propagation models," *IEEE Transactions on Antennas and Propagation*, vol. 65, no. 12, pp. 6213–6230, 2017.

[24] A. M. Al-Saman, M. Cheffena, M. Mohamed, M. H. Azmi, and Y. Ai, "Statistical analysis of rain at millimeter waves in tropical area," *IEEE Access*, vol. 8, pp. 51 044–51 061, 2020.

[25] R. S. of ITU, "Propagation data and prediction methods required for the design of terrestrial line-of-sight systems," International Telecommunications Union, Tech. Rep. P.530-17, 2017.

[26] R. Crane, "Prediction of attenuation by rain," *IEEE Transactions on Communications*, vol. 28, no. 9, pp. 1717–1733, 1980.

[27] "Fog types," https://www.weather.gov/source/zhu/ZHU_Training_Page/fog_stuff/fog_definitions/Fog_definitions.html.

[28] H. Wallace, "Millimeter-wave propagation measurements at the ballistic research laboratory," *IEEE Transactions on Geoscience and Remote Sensing*, vol. 26, no. 3, pp. 253–258, 1988.

[29] V. A. Golunov, A. V. Kuz'min, and G. I. Skulachev, D. P. ; Khokhlov, "Experimental results on the frequency dependence of attenuation, scattering, and absorption of millimeter waves in a dry snow cover," *Journal of Communications Technology and Electronics*, vol. 62, pp. 951–959, 2017.

[30] K. Nakamura, N. Iwasawa, K. Kawasaki, S. Yoshida, and M. Takahashi, "The attenuation characteristics of millimeter-wave by snow accretion," *IEICE Communications Express*, vol. 9, no. 12, pp. 674–678, 2020.

[31] F. Schwering, E. Violette, and R. Espeland, "Millimeter-wave propagation in vegetation: experiments and theory," *IEEE Transactions on Geoscience and Remote Sensing*, vol. 26, no. 3, pp. 355–367, 1988.

[32] S. Joshi and S. Sancheti, "Foliage loss measurements of tropical trees at 35 ghz," in *2008 International Conference on Recent Advances in Microwave Theory and Applications*, 2008, pp. 531–532.

[33] S. Rajagopal, S. Abu-Surra, and M. Malmirchegini, "Channel feasibility for outdoor non-line-of-sight mmwave mobile communication," in *2012 IEEE Vehicular Technology Conference (VTC Fall)*, 2012, pp. 1–6.

[34] S. Nie, G. R. MacCartney, S. Sun, and T. S. Rappaport, "72 ghz millimeter wave indoor measurements for wireless and backhaul communications," in *2013 IEEE 24th Annual International Symposium on Personal, Indoor, and Mobile Radio Communications (PIMRC)*, 2013, pp. 2429–2433.

[35] G. R. MacCartney and T. S. Rappaport, "73 ghz millimeter wave propagation measurements for outdoor urban mobile and backhaul communications in new york city," in *2014 IEEE International Conference on Communications (ICC)*, 2014, pp. 4862–4867.

[36] L. W. Couch, *Digital and Analog Communication Systems*. Pearson, 2013.

[37] W. F. Egan, *Practical RF system design.* Hoboken, New Jersey: Wiley-Interscience, 2004.

[38] C. A. Balanis, *Antenna theory analysis and design*, 4th ed. Hoboken, N.J: Wiley, 2016.

[39] M. I. Skolnik, *Introduction to Radar Systems.* McGraw-Hill, Inc., 1962.

[40] MathWorks, "polarpattern class," https://www.mathworks.com/help/antenna/ref/polarpattern-class.html?searchHighlight=polarpattern&s_tid=srchtitle.

[41] J. Sankar, "Antenna polarisation," https://www.electronicsforu.com/technology-trends/learn-electronics/antenna-polarisation, online: accessed 05-1-2021.

[42] P. McNeil, "Demystifying popular waveguide antennas for mmwave applications," *Microwave Journal*, vol. 63, no. 10, pp. 60–70, 2020.

[43] P. A. Rizzi, *Microwave Engineering Passive Circuits.* Englewood Cliffs, NJ: Prentice-Hall International, Inc, 1988.

[44] A. Boriskin and R. Sauleau, Eds., *Aperture Antennas for Millimeter and Sub-Millimeter Wave Applications*, 1st ed., ser. Signals and Communication Technology. Cham: Springer International Publishing, 2018.

[45] C. S. Vaucher, *Architectures for RF frequency synthesizers*, ser. The Kluwer international series in engineering and computer science Architectures for RF frequency synthesizers. Boston, MA: Springer US, 2002.

[46] R. Wallace and K. Andreasson, *Introduction to RF and Microwave Passive Components.* Norwood: Artech House, 2015.

[47] J. B. Hagen, *Radio-frequency electronics circuits and applications*, 2nd ed. Cambridge ;: Cambridge University Press, 2009.

[48] "Rf directional couplers and 3db hybrids overview," https://www.ieee.li/pdf/essay/directional_couplers.pdf.

[49] L. A. L. A. Belov, *Handbook of RF, microwave, and millimeter-wave components*, ser. Artech House microwave library. Boston ;: Artech House, 2012 - 2012.

[50] *ADMV7410-EVALZ User Guide*, Analog Devices, available at https://www.analog.com/media/en/technical-documentation/user-guides/ADMV7410-EVALZ-UG-1591.pdf, last accessed 04-29-2021.

[51] "Admv7410," https://www.analog.com/en/products/admv7410.html?doc=admv7410-evalz-ug-1591.pdfproduct-evaluationkit, online: accessed 04-29-2021.

[52] *E-Band Low Noise Downconverter SiP*, Analog Devices, available at https://www.analog.com/media/en/technical-documentation/data-sheets/ADMV7410.pdf, last accessed 04-29-2021.

[53] *Power Splitter/Combiner*, Mini-Circuits, available at https://www.minicircuits.com/pdfs/ZAPDJ-2-S+.pdf, last accessed 04-29-2021.

[54] *90 Degree SMA Hybrid Coupler from 1 GHz to 2 GHz Rated to 50 Watts*, Pasternack, available at https://www.pasternack.com/sma-coupler-2-ghz-pe2cp013-p.asp, last accessed 04-29-2021.

[55] *WR-12 Standard Gain Horn Antennas*, Millimeter Wave Products Inc., available at https://www.miwv.com/e-band-horn-antennas-wr-12-60-90-ghz/, last accessed 04-29-2021.

[56] *MLSP Series*, Micro Lambda Wireless, Inc, available at https://www.microlambdawireless.com/uploads/pdfs/MLSP-for-VSAT-datasheet.pdf, last accessed 04-29-2021.

[57] *RT-65series*, available at https://www.meanwell.com/productPdf.aspx?i=484, last accessed 04-29-2021.

[58] *RS-15 series*, Mean Well, available at https://www.meanwell.com/webapp/product/search.aspx?pr 15, last accessed 04-29-2021.

[59] *CSA Spectrum Analyzer N1996A*, Keysight Technologies, available at https:https://www.keysight.com/us/en/assets/7018-01320/brochures/5989-3678.pdf, last accessed 05-05-2021.

[60] *Toggle Switches*, NTE Electronics, Inc, available at https://www.nteinc.com/switches/pdf/toggle-std.pdf#page=10, last accessed 04-29-2021.

# Appendix A

# List of Components

**Components for Outdoor Testbed**

| Component | Quantity | Part Number | Company |
|---|---|---|---|
| Siklu Transceiver Radios | 4 | 73-EH-1200TX-ODU-EXT | Siklu |
| 1 foot Antennas | 4 | 73-EH-ANT-1FT-B | Alliance Communications |
| Power Over Ethernet Injector | 4 | 73-AX-MK-SP | Alliance Communications |
| Surge Protector | 4 | 73-PD-OUT/SP11 | Alliance Communications |

### Components for Measurement Platform

| **Components** | **Quantity** | **Part Number** | **Company** |
|---|---|---|---|
| Spectrum Analyzer | 1 | N1996A Agilent CSA (3GHz) | Agilent Technologies |
| Antenna | 1 | 261E-25/387 | Millimeter Wave Products Inc |
| Attenuator | 1 | PE70A1009 | Pasternack |
| 180 Degree Hybrid Coupler | 2 | ZAPDJ-2-S+ | Mini Circuits |
| 90 Degree Hybrid Coupler | 1 | PE2CP013 | Pasternack |
| | | | |
| **Power Supply** | | | |
| -5V Power Supply | 1 | RS-15-5 | Mean Well |
| 5V Power Supply | 1 | RS-15-5 | Mean Well |
| Frequency Synth. Power | 1 | RT-65C | Mean Well |
| Toggles | 4 | 54-738 | NTE Electronics, Inc. |
| | | | |
| **Connectors** | | | |
| SMA male to SMA male | 6 | PE34180LF-6 | Pasternack |
| 2.92mm to SMA adaptor | 1 | FMAD1187 | Fairview Microwave |
| Type N to SMA adaptor | 1 | NM-SF50+ | Mini Circuits |
| Long SMA Cables 8.5 ft | 2 | FMC0202085LF-90 | Fairview Microwave |

# Appendix B

# Measurement Platform Setup and Operation Steps

## B.1 Steps for Hardware Setup

**Connections from Downconverter outputs to spectrum analyzer:**

1. Connect the four 6inch SMA cables onto the four outputs of the downconverter (IF_QP, IF_QN, IF_IP, IF_IN)
2. Connect the two inputs of the 180 hybrid coupler to the IF_QP and IF_QN outputs on the downconverter
3. Connect the two inputs of the second 180 degree hybrid coupler to the IF_IP and IF_IN outputs on the downconverter
4. Connect the output of one of the 180 degree hybrid couplers to the IN port on the 90 degree hybrid coupler
5. Connect the output of the other 180 degree hybrid coupler to the ISOL port on the 90 degree hybrid coupler
6. Connect 7 ft SMA cable to the output labeled 90° on the 90 degree hybrid coupler

7. Connect the other end of the SMA cable from set 6 onto the SMA Male connector side of the 3 dB attenuator.
8. Connect the SMA Male connector on the attenuator with the SMA Female connector on the SMA Female to N Male adaptor
9. Connect the N Male side of the adaptor onto the N Female connector on the spectrum analyzer
10. Connect the 2.92mm Male side of the 2.92mm to SMA female adaptor on the LO input of the downconverter

**Connections from the Downconverter to the frequency synthesizer:**

11. Connect a 7 ft SMA cable onto the adaptor at the LO input
12. Connect the other end of the SMA cable in step 11 to the J4 on the frequency synthesizer
13. Place the DC Power wire harness and mating connector onto the J1 connector of the frequency synthesizer
14. Connect a wire to pin 1 on the J1 connector of the frequency synthesizer
15. Connect a wire to pin 2 on the J1 connector of the frequency synthesizer
16. Solder both of the wire ends from step 14 and step 16 onto the +V2 input on the 5V/15V power supply and label power supply 5V/15V

**Power Supply Set Up:**

17. Connect a wire to pin 5 on the J1 connector of the frequency synthesizer
18. Connect a wire to pin 6 on the J1 connector of the frequency synthesizer
19. Solder both of the wire ends from step 17 and step 18 onto the +V1 input on the 5V/15V power supply
20. Pick a wire color and solder a 7 ft wire onto the P5V on the downconverter

21. Connect this wire to the one of the 5V power supplies +V inputs and label power supply +5V
22. Take a 7 ft black wire and solder onto the GND on the downconverter that is right next to the P5V
23. Connect this wire to the -V input of the same power supply used in Step 21
24. Pick a different wire color than in step 21 and solder a 7 ft wire onto the NPV on the downconverter
25. Connect the wire, from the previous step, to the -V input onto the other 5V power supply (NOT the power supply from step 21) and label the power supply -5V
26. Take a 7 ft black wire and solder onto the GND on the downconverter that is right next to the N5V
27. Connect this wire to +V input of the same power supply used in Step 19
28. Take off the jumper connecting pin 1 and pin 2 on the J4 section on the downconverter
29. Connect a jumper with a wire attached onto pin 1
30. Connect a jumper with a wire attached onto pin 2
31. Solder the end of the wire from step 19 to one of the pins on a toggle
32. Solder the end of the wire from step 19 to the other pin on the same toggle as in step 21, label this toggle T3
33. Solder the black wire on a Unterminated AC Power Cord and onto one of the ends of a new toggle and label toggle -5V
34. On the other end of the toggle, from Step 33, solder another black wire
35. Connect the black wire from Step 34 onto the AC/L (pin 1) of the -5V power supply from step 25

36. Solder the green wire, of the power cord from step 33, onto the FG input on the -5V power supply from step 25

37. Solder the white wire, of the power cord from step 33, onto the AC/N (pin 1) of the -5V power supply from step 25

38. Take a different Unterminated AC Power cord and solder its black wire onto one of the ends of a new toggle and label toggle +5V

39. Solder another black wire on the other end of the toggle from Step 38 and label toggle +5V

40. Connect the black wire from Step 39 on to the AC/L (pin 1) of the +5V power supply from step 21

41. Solder the green wire, of the power cord from step 38, onto the FG input on the +5V power supply from step 21

42. Solder the white wire, of the power cord from step 38, onto the AC/N (pin 1) on the +5V power supply from step 21

43. Take a different Unterminated AC Power cord and solder its black wire onto one of the ends of a new toggle and label toggle 15V

44. Solder another black wire on the other end of the toggle from Step 43

45. Connect the black wire from Step 44 on to the AC/L (pin 1) of the 5V/15V power supply from step 16

46. Solder the green wire, of the power cord from step 43, onto the FG input on the 5V/15V power supply from step 16

47. Solder the white wire, of the power cord from step 43, onto the AC/N (pin 1) on the 5V/15V power supply from step 16

48. Turn all toggles to the “OFF” position

49. Plug in the AC power cord plus sides from steps 33, 38, and 43 onto a power strip with 1 plug that will go to an external power source
50. Plug in the spectrum analyzer to the same power strip as in step 49

**Final Steps**

51. Connect the antenna onto the downconverter matching the waveguide opening configuration
52. Connect a USB Mini B onto the J2 input on the frequency synthesizer
53. Connect the other end of the USB to a laptop
54. Take the CD ROM that came with the frequency synthesizer and insert it into a PC running windows
55. Execute the SetupMLSP.msi file

## B.2 Steps for Operation

1. Turn all toggles to the "OFF" position
2. Connect the external power plug of the power strip
3. Flip the -5V toggle to the "ON" position
4. Wait 1 minute
5. Flip the 5V toggle to the "ON" position
6. Wait 1 minute
7. Flip the T3 toggle to the "ON" position
8. Wait 1 minute
9. Flip the 15V toggle to the "ON" position
10. Wait 5 minutes for frequency synthesizer to warm up

11. Ensure the laptop and USB connection to the frequency synthesizer is secure.

12. On the laptop click the MLSP PC interface.exe program

13. Select the appropriate frequency for the LO input based on the desired center frequency of the Siklu Radios. The following table is a guide for choosing the LO frequency when the channel bandwidth is set to 125 MHz and the desired IF frequency is 1500 MHz.

| Channel Center Freq (MHz) | IF Freq (MHz) | LO Freq (MHz) |
|---|---|---|
| 71937.5 | 1500 | 11739.6 |
| 72062.5 | 1500 | 11760.4 |
| 72187.5 | 1500 | 11781.3 |
| 72312.5 | 1500 | 11802.1 |
| 72437.5 | 1500 | 11822.9 |
| 72562.5 | 1500 | 11843.8 |
| 72687.5 | 1500 | 11864.6 |
| 72812.5 | 1500 | 11885.4 |
| 72937.5 | 1500 | 11906.3 |
| 73062.5 | 1500 | 11927.1 |
| 73187.5 | 1500 | 11947.9 |
| 73312.5 | 1500 | 11968.8 |
| 73437.5 | 1500 | 11989.6 |
| 73562.5 | 1500 | 12010.4 |
| 73687.5 | 1500 | 12031.3 |
| 73812.5 | 1500 | 12052.1 |
| 73937.5 | 1500 | 12072.9 |
| 74062.5 | 1500 | 12093.8 |
| 74187.5 | 1500 | 12114.6 |
| 74312.5 | 1500 | 12135.4 |
| 74437.5 | 1500 | 12156.3 |

| | | |
|---|---|---|
| 74562.5 | 1500 | 12177.1 |
| 74687.5 | 1500 | 12197.9 |
| 74812.5 | 1500 | 12218.8 |
| 74937.5 | 1500 | 12239.6 |
| 75062.5 | 1500 | 12260.4 |
| 75187.5 | 1500 | 12281.3 |
| 75312.5 | 1500 | 12302.1 |
| 75437.5 | 1500 | 12322.9 |
| 75562.5 | 1500 | 12343.8 |
| 75687.5 | 1500 | 12364.6 |

14. SSH into the appropriate server that the Siklu radio you will be measuring is on using the command "ssh username@IP_addr_of_computer"
15. SSH into the siklu radio via "ssh admin@192.168.n.2", where n is the radio number
16. Password is "admin"
17. Input command "show rf" to check the center frequency and the channel width of the Radios
18. Type command "exit"
19. Turn on the Spectrum analyzer
20. SSH into the receiver side of the communication link you wish to measure and input command "iperf3 -s -B 192.168.n.1" , where n is the radio number
21. Put the antenna of the downconverter in line with the transmit antenna
22. SSH into the transmitter side of the communication link (the radio you will be measuring emissions from) and input command "iperf3 -c 192.168.n.1 -t 20", where n is the radio number

a. The 20 seconds can also be changed to however long you want the data to be transmitting in seconds

23. Auto configure spectrum analyzer to see the signal
24. Make measurements
25. Disconnect the laptop from frequency synthesizer item
26. Flip the 15V Toggle to the “OFF” position
27. Wait 5 minutes for frequency synthesizer to power down
28. Flip the T3 Toggle to the “OFF” position
29. Flip the 5V Toggle to the “OFF” position
30. Flip the -5V Toggle to the “OFF” position
31. Turn off the iperf3 server
32. Disconnect from the servers using command “exit”